



## A covalent strategy to target intrinsically disordered proteins: Discovery of novel tau aggregation inhibitors



László Petri<sup>a,1</sup>, Péter Ábrányi-Balogh<sup>a,1</sup>, Dariusz Vagrys<sup>a,b,c</sup>, Tímea Imre<sup>a,d</sup>, Nikolett Varró<sup>e</sup>, István Mándity<sup>e</sup>, Anita Rácz<sup>a,f</sup>, Lucia Wittner<sup>g</sup>, Kinga Tóth<sup>g</sup>, Estilla Zsófia Tóth<sup>g</sup>, Tünde Juhász<sup>h</sup>, Ben Davis<sup>b</sup>, György Miklós Keserű<sup>a,\*</sup>

<sup>a</sup> Medicinal Chemistry Research Group, Research Centre for Natural Sciences, Magyar Tudósok krt 2, 1117, Budapest, Hungary

<sup>b</sup> Vernalis Research, Granta Park, Great Abington, Cambridge, CB21 6GB, United Kingdom

<sup>c</sup> York Structural Biology Laboratory, University of York, Heslington, York YO10 5DD, United Kingdom

<sup>d</sup> MS Metabolomics Research Group, Research Centre for Natural Sciences, Magyar Tudósok krt 2, 1117, Budapest, Hungary

<sup>e</sup> Artificial Transporters Research Group, Research Centre for Natural Sciences, Magyar Tudósok krt 2, 1117, Budapest, Hungary

<sup>f</sup> Plasma Chemistry Research Group, Research Centre for Natural Sciences, Magyar Tudósok krt 2, 1117, Budapest, Hungary

<sup>g</sup> Integrative Neuroscience Research Group, Research Centre for Natural Sciences, Magyar Tudósok krt 2, 1117, Budapest, Hungary

<sup>h</sup> Biomolecular Self-Assembly Research Group, Research Centre for Natural Sciences, Magyar Tudósok krt 2, 1117, Budapest, Hungary

### ARTICLE INFO

#### Article history:

Received 15 December 2021

Received in revised form

17 January 2022

Accepted 26 January 2022

Available online 29 January 2022

#### Keywords:

Electrophilic warhead

Covalent inhibition

Tau aggregation

Tauopathy

### ABSTRACT

Intrinsically disordered proteins (IDPs) play important roles in disease pathologies; however, their lack of defined stable 3D structures make traditional drug design strategies typically less effective against these targets. Based on promising results of targeted covalent inhibitors (TCIs) on challenging targets, we have developed a covalent design strategy targeting IDPs. As a model system we chose tau, an endogenous IDP of the central nervous system that is associated with severe neurodegenerative diseases via its aggregation. First, we mapped the tractability of available cysteines in tau and prioritized suitable warheads. Next, we introduced the selected vinylsulfone warhead to the non-covalent scaffolds of potential tau aggregation inhibitors. The designed covalent tau binders were synthesized and tested in aggregation models, and inhibited tau aggregation effectively. Our results revealed the usefulness of the covalent design strategy against therapeutically relevant IDP targets and provided promising candidates for the treatment of tauopathies.

© 2022 The Author(s). Published by Elsevier Masson SAS. This is an open access article under the CC BY license (<http://creativecommons.org/licenses/by/4.0/>).

### 1. Introduction

Targeted covalent inhibitors (TCIs) have recently become important chemical biological tools and evaluated in specific drug discovery programs [1–4]. These compounds form a permanent covalent bond with an appropriate nucleophilic residue (most often cysteine, but also others, including lysine, serine, threonine and tyrosine) of the target protein [5]. Covalent binding makes ligand discovery feasible against challenging binding sites such as protein-protein interactions [6], allosteric pockets [7] and high affinity sites specific for endogenous partners such as transcription factors [8] or small GTPases [9].

Intrinsically disordered proteins (IDPs) play important roles in

the regulation of cellular functions, and thus they represent potential therapeutic targets. These proteins, however, lack a well-defined 3D structure, and rather exist as an ensemble of highly dynamic conformations [10,11]. This feature makes IDPs challenging to drug by classical approaches. Recent promising experience with TCIs prompted us to develop a covalent strategy against this important class of drug targets. Our preliminary experiments with a human IDP, calpastatin revealed that it can be specifically labelled by covalent fragments that blocked its protein-protein interaction with the calcium-dependent cysteine protease calpain [12]. In this work we report a protocol for developing covalent inhibitors against IDPs that is exemplified by the aggregation-prone tau protein that is involved in multiple tauopathies, including Alzheimer's disease [13–16]. Tau aggregates, found in brain tissue, exhibit increased levels of phosphorylation and mostly contain double helical stacks, or paired helical filaments (PHFs) [17]. It has been demonstrated that two hexapeptide motifs (Fig. 1) PHF6

\* Corresponding author.

E-mail address: [keseru.gyorgy@ttk.hu](mailto:keseru.gyorgy@ttk.hu) (G.M. Keserű).

<sup>1</sup> These authors contributed equally.

(VQIVYK) and PHF6\* (VQIINK) are involved in the formation of PHFs and are found at the core of formed fibrils [18–20].

Because of the importance of PHF6 (VQIVYK) and PHF6\* (VQIINK) regions in fibril formation, tau-K18 construct, containing 4 repeat regions (R1–R4), has been used extensively as a model system in order to identify and evaluate aggregation inhibitors [21–27]. Covalent tau ligands, however, appear only occasionally in literature, mostly discovered serendipitously and heuristically [28–33].

Design principles for TCIs have expanded substantially in recent years, as many studies have already described advantages and disadvantages of these inhibitors [34,35]. The reactivity and specificity of TCIs have major impacts on their therapeutic utility and should therefore be specifically tailored to the target [36]. Since the local environment of the targeted protein nucleophile influences substantially its reactivity and accessibility [37,38], rational selection of the warhead moiety is of the utmost importance [39,40]. Using covalent fragment screening [41,42], we recently introduced an experimental optimization protocol [41] that has already been proven in target-specific warhead selection for covalent drug discovery programs [43,44]. These data confirmed that screening a specific mapping library of electrophilic functionalities equipped to the same fragment scaffold might identify suitable warheads for a particular target.

Our strategy for covalent IDP-inhibitors involves two major steps: selection of suitable electrophilic functionalities by covalent fragment screening and the use of these electrophiles as warheads on non-covalent scaffolds [44]. First, we evaluated the covalent tractability of tau and confirmed that tau oligomer formation can be inhibited by appropriate covalent labelling of the monomer. Next, we designed, synthesized and tested covalent aggregation inhibitors carrying the optimized warhead. A range of biophysical techniques and orthogonal methods were used to characterize and explore the interactions between monomeric tau-K18 and designed covalent ligands. Finally, we demonstrated that the design strategy we introduce here can lead us to efficient covalent binders inhibiting tau filament formation. We believe that this concept can open new perspectives for the rational design of covalent inhibitors for other IDPs with therapeutic significance.

## 2. Results and discussion

### 2.1. Rational warhead selection

Covalent inhibitor design demands proper selection of the warheads tailored to the specific target. To evaluate the reactivity profile of tractable cysteines in tau protein (C291 and C321) we tested the tau-K18 construct (hereafter tau-K18<sup>WT</sup>) and our covalent mapping library (1–25, Fig. 2a) used successfully for warhead optimization in earlier studies [43,44]. We evaluated covalent

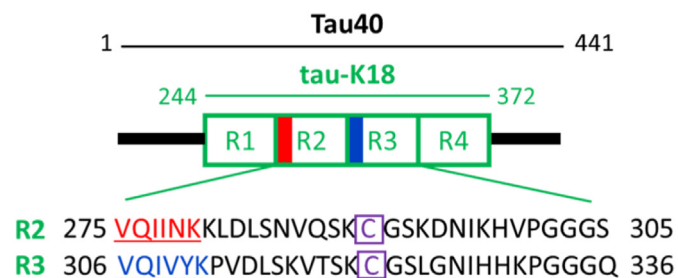


**Fig. 1.** Full-length tau (Tau40). Depicting sequence alignment of R2 and R3 subunits from Tau40 including the positions of PHF6 (VQIVYK) (blue) and PHF6\* (VQIINK) (red) segments in the K18 domain (green), moreover the position of covalently vulnerable C291 and C322 cysteines (purple) are also shown here.

tractability using orthogonal biochemical and biophysical methods, namely the fluorescence-based Ellman's assay, intact protein MS and ligand observed <sup>19</sup>F NMR measurements, to determine the labelling efficiency. For the Ellman's assay, we applied a 50% threshold for the remaining free thiol ratio after labelling since tau has two available cysteines to be modified, and thus, complete labelling of one cysteine could result in 50% labelling ratio (LR%). Intact protein MS measurements are routinely used for covalent fragment screening. Our mapping library, however, is specifically designed for ligand observed <sup>19</sup>F NMR evaluation of covalent binding as warheads are applied on a fluorine-rich scaffold (3,5-bis(trifluoromethyl)phenyl) [43].

Based on the orthogonal mapping results (Fig. 2b) we selected 3 probes identified as positive hit by all the three methods (Ellman's assay, MS and <sup>19</sup>F NMR). Mapping fragments **6**, **10** and **11** equipped with the maleimide, ethynyl ester and vinylsulfone warheads respectively labelled the tau cysteines effectively. The maleimide probe was deprioritized due to its low aqueous stability [44] and promiscuous reactivity [45]. Next we compared fragments **10** and **11**, where the ethynyl ester (**10**) showed higher reactivity, but still, only moderate aqueous stability as compared to the vinylsulfone probe (**11**) [43]. Thus, we selected the vinylsulfone warhead (**11**) for the development of covalent tau aggregation inhibitors and confirmed labelling at both cysteines of tau-K18<sup>WT</sup> by <sup>15</sup>N-HSQC NMR experiments (Fig. 2c).

### 2.2. Development for covalent aggregation inhibitors

We then used the vinylsulfone warhead on a range of non-covalent scaffolds to identify novel aggregation inhibitors with covalent mechanism of action. These scaffolds were based on a set of proposed or experimentally confirmed non-covalent tau aggregation inhibitors. Starting from the binding sites suggested for non-covalent tau ligands we selected 4 prototypical scaffolds having binding sites (Fig. 3) proximal to the targeted cysteines (C291 and C322) [21,46–48].

Our intention was to anchor the scaffolds close to the PHF6\* and PHF6 regions, which could then interfere with the conformation required for aggregation. The specific residues involved in non-covalent interactions of the scaffolds are discussed below in the section of describing individual concepts. The diversity of the approaches demonstrated herein shows that various IDP drug discovery programs can be merged with the concept of covalent targeting (Fig. 4a–e).

#### 2.2.1. Hydrophobic vinylsulfones (Fig. 4a; **11**, 26–33)

It has been suggested that C322 and C291 can stabilize the aggregated conformation of tau and moreover that these residues can initiate the aggregation process [49]. Steric clashes close to the PHF6 and PHF6\* regions resulting from the covalent ligation of the cysteines might therefore block the aggregation process. The hydrophobic pocket formed inside the tau hairpin conformation [23] suggested that the cysteine reactive warhead should be presented on hydrophobic scaffolds with different size and complexity in order to optimize non-covalent interactions. Our set (**11**, 26–33) included fragments with hydrophobic aromatic and aliphatic rings (Fig. 4a), including the original fragment hit **11**.

#### 2.2.2. Rhodanine-based vinylsulfone (Fig. 4b; **34**)

Rhodanines have been described previously as potential tau aggregation inhibitors [50]. It is proposed that this chemotype binds to glutamine Q307 and lysine K311 via hydrogen bonding (Fig. 3) and blocks the aggregation [46]. The mode of action of this compound class is, however, still poorly understood. Taking the advantage of the specific labelling of nearby cysteine residues we

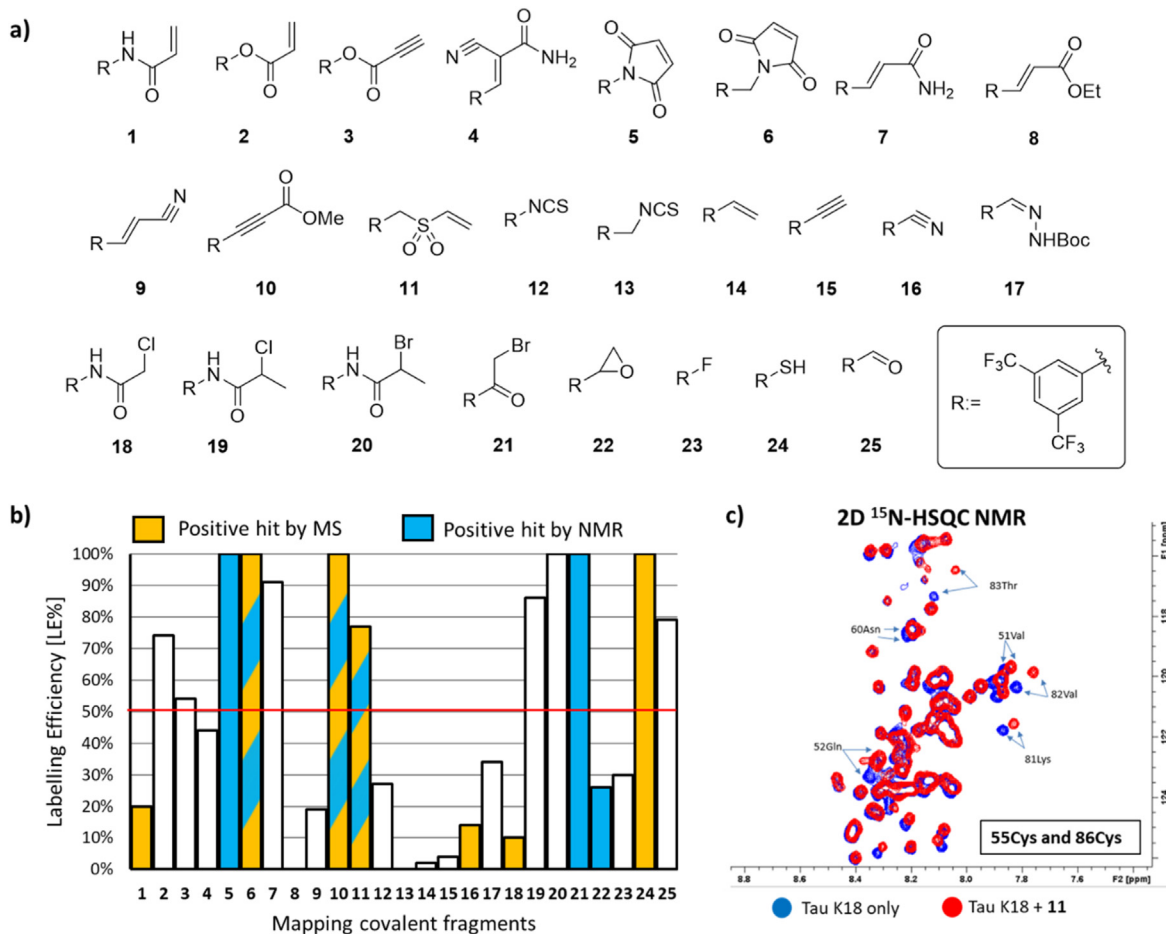


**Fig. 2.** a) Specific covalent fragment library (1–25) for warhead optimization. b) Results of orthogonal analytical methods (Ellman's assay, MS and <sup>19</sup>F NMR) for covalent labelling. The histogram shows Labelling Efficiency (LE%) resulted by the Ellman's assay. The red line shows the threshold for the Ellman's assay results and the bars are colored according to the results of the MS- and ligand observed NMR-based screens, as follows: empty bars represent covalent probes not resulted as positive hit in any of the MS- or ligand observed NMR-based assays; yellow bars represent covalent probes resulted as positive hit in the MS-based assay; blue bars represent covalent probes resulted as positive hit in the ligand observed NMR-based assay and bicoloured bars represent the covalent probes resulted as positive hit in both assay. c) Vinylsulfone **11** binds to both of the cysteine residues of tau-K18<sup>WT</sup> as revealed by <sup>15</sup>N-HSQC NMR experiments.

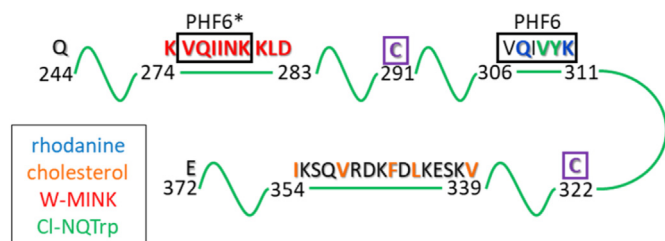


**Fig. 3.** Binding regions of tau-K18<sup>WT</sup>. Affected residues are colored as follows: blue letters for rhodanine, orange letters for cholesterol, red letters for W-MINK and green letters for CI-NQTrp-based peptide.

prepared the rhodanine scaffold with a vinylsulfone warhead (**34**, Fig. 4b).

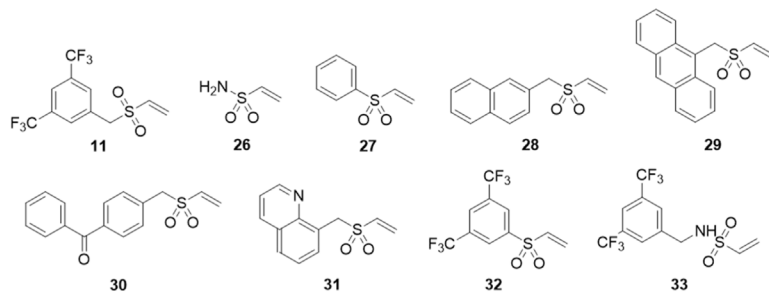
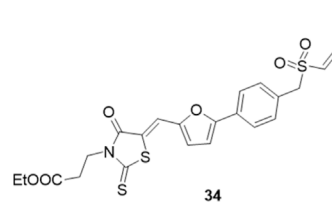
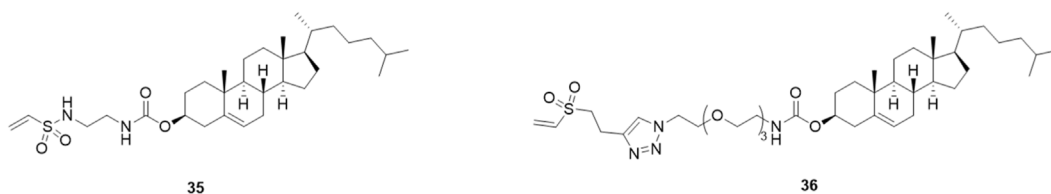
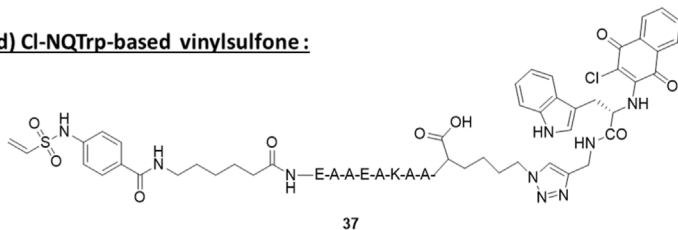
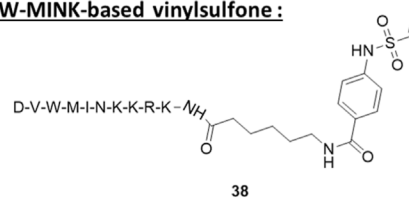
### 2.2.3. Cholesterol-based vinylsulfones (Fig. 4c; **35**, **36**)

Sterols have been reported [47,51] as promising aggregation inhibitors and therefore, we prepared cholesterol with the vinylsulfone warhead (**35**, Fig. 4c). In addition, to accommodate conformational flexibility and the distance between the proposed cholesterol-binding site [47]—surrounded by the hydrophobic side chains of V339, L344, F346, V350 and I354 (Fig. 3)—and the

targeted cysteines, another analogue with a longer PEG-linker was also synthesized (**36**, Fig. 4c).

### 2.2.4. Chloronaphthoquinone-tryptophan-based vinylsulfone (Fig. 4d; **37**)

Chloronaphthoquinone (Cl-NQ) coupled to tryptophan (Cl-NQTrp) has been shown recently to bind to tau-K18<sup>M</sup> monomer contacting residues V309 and Y310 within the PHF6 region (Fig. 3) [21]. Thus, we designed a covalently reactive derivative (**37**, Fig. 4d). The vinylsulfone tail was attached to the Cl-NQTrp head via a decapeptide linker with suitable polarity and length to ensure conformational flexibility and to reach to the targeted cysteines. To prevent peptide N-termini and C-terminal lysine residues from crosslinking, two modified residues were incorporated into the peptide: at C-terminal an  $\epsilon$ -azido-L-lysine, which then was clicked onto the Cl-NQTrp head-structure; and 6-Ahx (6-aminocaproic acid) was introduced at the N-termini of the peptide, and then acylated by the vinylsulfone warhead bearing tail-structure. Within the linker sequence glutamic acid, alanine and lysine residues were incorporated [52–55]. The peptide was synthesized on Tentagel® resin applying Fmoc chemistry [56].

**a) Library of hydrophobic vinylsulfones:****b) Rhodanine-based vinylsulfone:****c) Cholesterol-based vinylsulfones:****d) Cl-NQTrp-based vinylsulfone:****e) W-MINK-based vinylsulfone:**

**Fig. 4.** Designed covalent tau inhibitors: **a)** hydrophobic vinylsulfone library (**11, 26–33**); **b)** rhodanine-based vinylsulfone derivative (**34**); **c)** cholesterol-based vinylsulfone derivatives (**35, 36**); **d)** naphthoquinone-tryptophan-headed peptide equipped with a vinylsulfone warhead (**37**) and **e)** W-MINK peptidic inhibitor equipped with a vinylsulfone warhead (**38**).

### 2.2.5. Peptide (W-MINK)-based vinylsulfone (Fig. 4e; 38)

A structure-based design strategy recently resulted in peptide-like aggregation inhibitors [57]. The most active decapeptide W-MINK was found to inhibit the aggregation of the full-length tau effectively. This peptide formed non-covalent interactions with residues of the K274–D283 segment (Fig. 3), which includes the PHF6\* sequence region (V275–K280) [57]. Therefore, we prepared this decapeptide with the vinylsulfone warhead (Fig. 4e) designed to anchor the peptide close to the aggregation region.

### 2.3. Influencing tau aggregation via covalent inhibitors

In order to investigate the effect of proposed covalent aggregation inhibitors, we followed the aggregation of vinylsulfone treated and untreated tau-K18<sup>WT</sup> in the ThT-based fluorescence assay [58,59]. Non-equilibrium covalent labelling of the target ensured that the final level of fluorescence could be related directly to the rate of aggregation inhibition. We first treated tau-K18<sup>WT</sup> with 50 eq. of the inhibitors, equal to 10  $\mu$ M assay concentration. Tau aggregation was initiated by heparin after incubation. The progression of tau aggregate formation was followed by adding ThT and monitoring the fluorescence signal (Fig. 5a). Aggregation rates (Supplementary Table S1) were determined as the fluorescence ratio compared to the untreated but aggregated tau-K18. After preliminary screening **11** and **29** hydrophobic vinylsulfones, rhodanine-derivative **34**, the **35** and **36** cholesterol vinylsulfones, the **37** Cl-NQTrp-derivative and the **38** W-MINK-vinylsulfone decreased aggregate ratios (Fig. 5b). These results demonstrated

the effectiveness of our strategy, as all the five design pathways led to potent covalent aggregation inhibitors.

To prove covalent binding mechanism of the designed inhibitors we performed the same experiments with a mutant tau-K18 construct (hereafter tau-K18<sup>M</sup>) [60]. Mutation of C291 and C322 to serine (C291S, C322S) is known to maintain similar protein-protein and protein-ligand interactions, but the cysteine selective vinyl sulfone warhead is not able to react with serine [21]. Control measurements with tau-K18<sup>M</sup> revealed (Fig. 5b) that the aggregation ratio is much lower in the absence of tractable cysteines. The impact of covalent binding was further investigated comparing the effect of non-covalent W-MINK peptide to that of its vinylsulfone analogue **38** (Fig. 5b). We found, that **38** performed better in the presence of cysteines ( $19 \pm 5\%$  of aggregation on tau-K18<sup>WT</sup> compared to  $43 \pm 9\%$  on tau-K18<sup>M</sup>). Contrary, non-covalent W-MINK control experiments showed similar inhibition with tau-K18<sup>WT</sup> ( $38 \pm 3\%$ ) and with tau-K18<sup>M</sup> ( $29 \pm 8\%$ ). Thus, we concluded that covalent binding contributes significantly to the inhibitory activity of the ligands.

Direct covalent binding of the designed compounds (**11, 26–38**) was tested in the Elmann's assay. Tau labelling was confirmed according to the measured free thiol ratios in the range of 22%–66% (Fig. 5c, Supplementary Table S2). We found that all effective inhibitors showed direct cysteine ligation. Moreover, we performed concentration-dependent analysis of aggregation inhibitory effect with 3 representative compounds (**11, 29, 4**) (Fig. 5d, Supplementary Table S3) and confirmed that their efficacy is directly controlled by the concentration of the inhibitors. Finally, the covalent mode of action was demonstrated by MS/MS

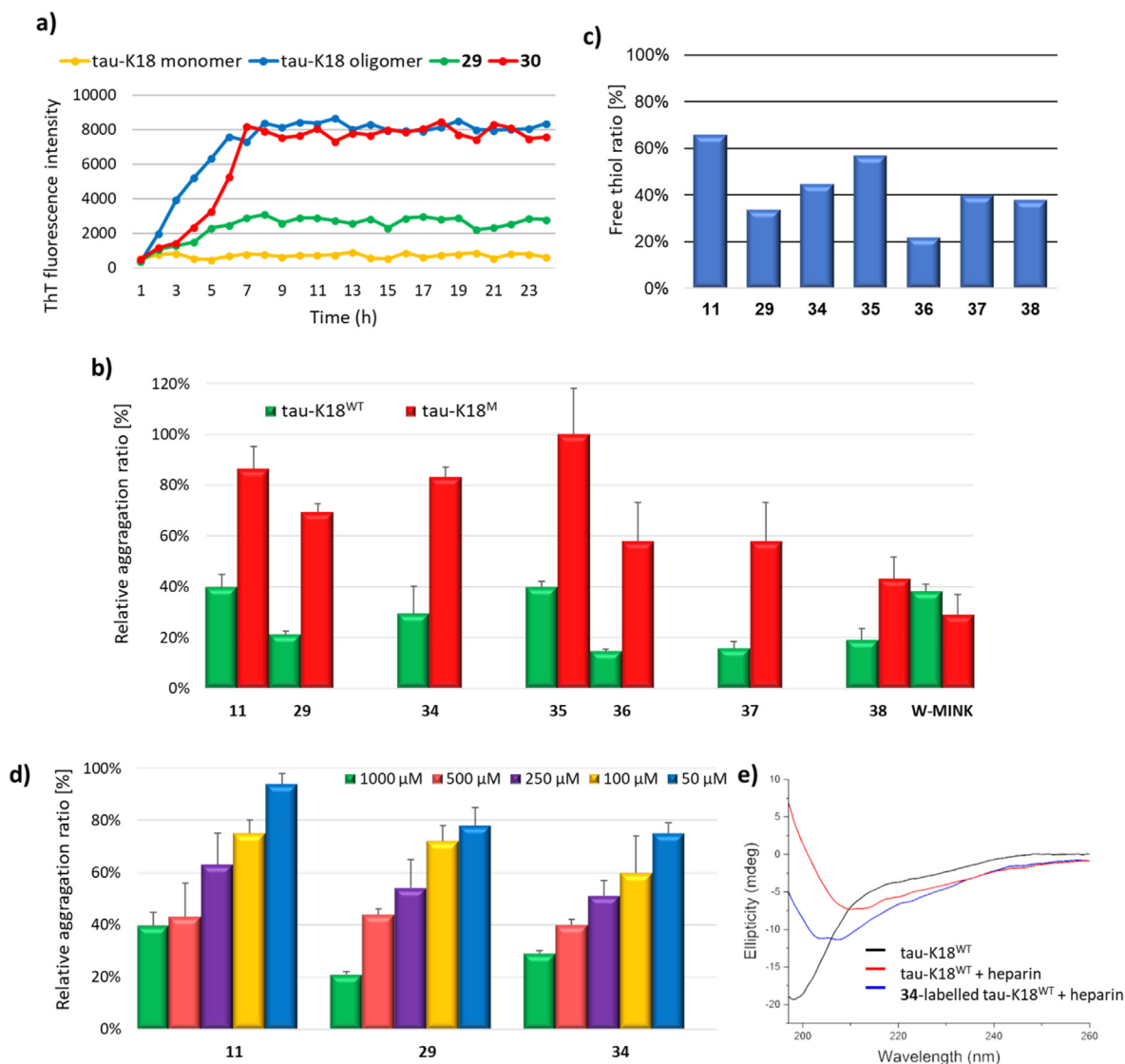


**Fig. 5.** a) Representation of the effect of small molecule inhibitors on the tau aggregation using ThT fluorescent additive. The graph shows the aggregated control (blue), the non-aggregated control (yellow), a case of effective inhibition (**29**, green) and a case of ineffective inhibition (**30**, red). b) The obtained aggregation ratios of the active inhibitors of tau-K18<sup>WT</sup> aggregation (green), in comparison with the effect obtained for the tau-K18<sup>M</sup> aggregation (red). Here we show also the results obtained by treating of tau-K18<sup>WT</sup> and tau-K18<sup>M</sup>, both, with the control compound W-MINK. c) Results of Ellman's assay of tau-K18<sup>WT</sup>. The Ellman's assay results are presented as free thiol ratio (FTR%), the percentage ratio of the unlabelled cysteines. d) Concentration-dependence of aggregation inhibition with probes **11**, **29** and **34** by 1000 μM (green), 500 μM (pink), 250 μM (purple), 100 μM (yellow) and 50 μM (blue), respectively. e) Circular dichroism (CD) spectrometry results showing the conformational changes of the tau during the heparin-induced aggregation (red) and the effect of **34** covalent probe (blue) compared to the monomer of tau-K18<sup>WT</sup> (black).

proteomics of tau-K18<sup>WT</sup> monomer labelled with **11**, **29** and **37** covalent probes. These measurements revealed that double labelling occurs at both C291 and C322 with **11** and **29**, however **37** labelled only at C291 (Supplementary Fig. S1 and Table S4).

Next, we investigated structural changes which occurred upon covalent labelling. Circular dichroism (CD) revealed that untreated tau-K18<sup>WT</sup> (black curve, Fig. 5e) was in a random coil conformation with a minimum in the CD spectrum at 200 nm, suggesting the presence of tau-K18<sup>WT</sup> monomers. After heparin-induced aggregation, the structure was shifted into  $\beta$ -sheet rich conformation (red curve, Fig. 5e), as evidenced by a minimum at 215 nm and a positive band at 198 nm. After applying the same aggregation protocol but having previously treated tau-K18<sup>WT</sup> with **34** (blue curve, Fig. 5e), the intensity at 215 nm was reduced, and the minimum of the spectra was shifted towards the random coil conformation range.

Supramolecular structural changes were investigated by transmission electron microscopy (TEM) analysis (Fig. 6) to demonstrate the tau oligomer fibrils formed after heparin-induced aggregation. In contrast to the unaggregated tau-K18<sup>WT</sup> monomer the TEM images (Fig. 6a) clearly show the progress of the aggregation. According to TEM results, we concluded that incubation of tau-K18<sup>WT</sup> with covalent probes could inhibit the aggregation with different efficacy. TEM images of the aggregated tau-K18<sup>WT</sup> in the absence of the inhibitors resulted in highly populated fibrils, indicating the formation of amyloids. Here we investigated the **35** and **36** cholesterol-derivatives and the Cl-NQTrp peptidic vinylsulfone (**37**). The micrographs were semi-quantitatively analyzed using ImageJ® software. After background subtraction, TEM images were compared according to their average brightness (Fig. 6b and Supplementary Table S5). Here the higher brightness implies the less aggregates formed. These results show that numbers of fibrils

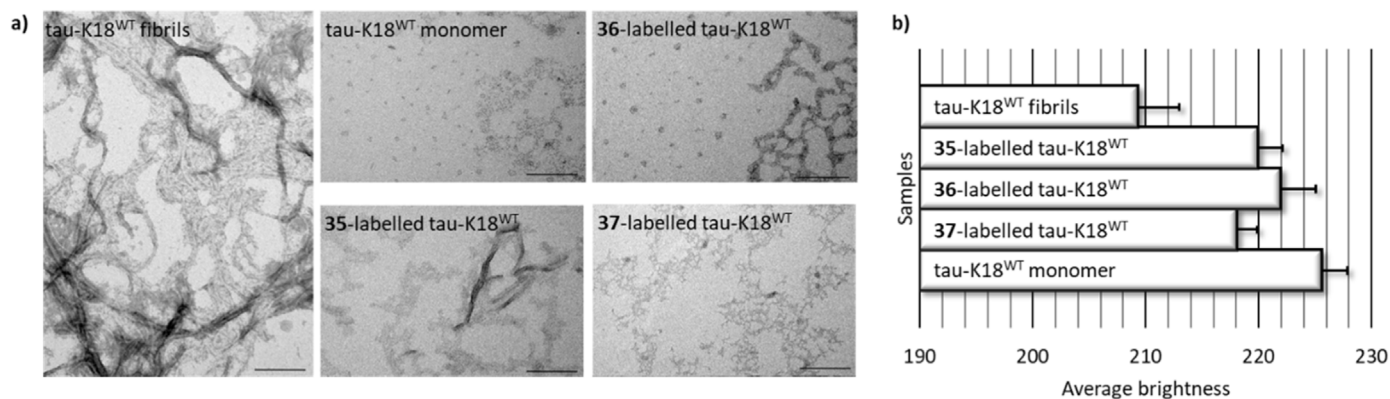


**Fig. 6.** a) High magnification ultra-micrographs of tau protein (scale: 100 nm). The heparin-induced aggregation resulted in high number of fibrils, contrasted by the image obtained by the non-aggregated monomer, and TEM images obtained after aggregation of **37**, **38** and **39**-labelled tau-K18<sup>WT</sup>. b) The semi-quantitative evaluation according to the average brightness of the TEM images.

formed by aggregation of tau-K18<sup>WT</sup> considerably decreased, thus, despite of the forced aggregation process tau-K18<sup>WT</sup> is mostly in monomer conformation.

### 3. Conclusion

Here we described a novel strategy to identify covalent ligands targeting intrinsically disordered protein targets. The approach was exemplified on tau protein and included the target-specific selection of an electrophilic warhead for labelling of the IDP. After covalent fragment screening against tau-K18 we showed that experimental reactivity information provides practical guidance for the prioritization of appropriate warhead chemotypes. Next, the prioritized vinylsulfone warhead was applied on different non-covalent scaffolds to design and synthesize potential covalent aggregation inhibitors. Testing these compounds in orthogonal methods confirmed their covalent mechanism of action by counter-screens on double mutant tau-K18<sup>M</sup> (C291S, C322S). We demonstrated that the designed covalent inhibitors induce conformational changes of tau that contribute to reduction of the macroscopic aggregation of tau fibrils. These results might represent opportunities for developing therapeutics against tauopathies, and moreover, the approach presented herein could be a useful strategy targeting other therapeutically relevant IDPs.

## 4. Experimental section

### 4.1. Protein expression and purification

Tau K18<sup>M</sup> and tau K18<sup>WT</sup> constructs were expressed and purified as described earlier [21]. All protein purification buffer solutions for tau K18<sup>WT</sup> construct contained 1 mM monothio glycerol (MTG), whereas the final size exclusion/storage buffer solution contained 2 mM DTT.

### 4.2. Ellman's assay

To measure thiol-reactivity, 2  $\mu$ M tau-K18<sup>WT</sup> in assay buffer (25 mM NaPi, 0.1 mM EDTA, 150 mM NaCl, pH 6.6) was treated with 200  $\mu$ M of fragments, resulting 5% DMSO concentration in the mixture. After 24 h of incubation on room temperature, 16  $\mu$ L of the sample was pipetted into a black, 384 well assay plate (Corning, Ref No.: 4514) and 4  $\mu$ L of thiol detection reagent (Invitrogen, Ref No.: TC012-1 EA) was added. After brief shaking, the plate was incubated in dark, room temperature for 30 min, then fluorescence was

measured in duplicates in a microplate reader (BioTek Synergy Mx) ( $\lambda_{\text{ex}} = 390$  nm and  $\lambda_{\text{em}} = 510$  nm). Free thiol ratio (FTR%) and labelling ratio (LR%) values were calculated, as follows:

$$\text{FTR}[\%] = 100 \cdot \frac{\text{RFU}_{\text{sample}} - \text{RFU}_{\text{background}}}{\text{RFU}_{\text{DMSO}} - \text{RFU}_{\text{background}}}$$

$$\text{LR}[\%] = 100\% - \text{FTR}[\%]$$

### 4.3. Protein labelling for tau-K18

For the tau-K18<sup>WT</sup> labelling experiments the 20  $\mu$ M stock solution of the protein (25 mM NaPi, 0.1 mM EDTA, 150 mM NaCl, pH 6.6) was treated with fragments added from a 100 mM DMSO stock diluted in the labelling solution to 1 mM. The incubation was continued at 25  $^{\circ}$ C for additional 24 h. After the labelling, the mixture directly submitted to MS analysis.

For NMR experiments, 50  $\mu$ M of tau K18<sup>WT</sup> was incubated with 250  $\mu$ M of covalent fragment in 50 mM NaPi, pH 6.6, 25 mM NaCl, 50  $\mu$ M DSS, 4% DMSO-*d*<sub>6</sub>, 5% D<sub>2</sub>O for 18 h at 25  $^{\circ}$ C.

### 4.4. MS analysis of the labelled tau-K18

The molecular weights of the conjugates of tau were identified using a Triple TOF 5600+ hybrid Quadrupole-TOF LC/MS/MS system (Sciex, Singapore, Woodlands) equipped with a DuoSpray IonSource coupled with a Shimadzu Prominence LC20 UFLC (Shimadzu, Japan) system consisting of binary pump, an autosampler and a thermostated column compartment. Data acquisition and processing were performed using Analyst TF software version 1.7.1 (AB Sciex Instruments, CA, USA). Chromatographic separation was achieved on a Thermo Beta Basic C8 (50 mm  $\times$  2.1 mm, 3  $\mu$ m, 150  $\text{\AA}$ ) HPLC column. Sample was eluted in gradient elution mode using solvent A (0.1% formic acid in water) and solvent B (0.1% formic acid in ACN). The initial condition was 20% B for 1 min, followed by a linear gradient to 90% B by 4 min, from 5 to 6 min 90% B was retained; and from 6 to 6.5 min back to initial condition with 20% eluent B and retained from 6.5 to 9.0 min. Flow rate was set to 0.4 ml/min. The column temperature was 40  $^{\circ}$ C and the injection volume was 5  $\mu$ L. Nitrogen was used as the nebulizer gas (GS1), heater gas (GS2), and curtain gas with the optimum values set at 30, 30 and 35 (arbitrary units), respectively. Data were acquired in positive electrospray mode in the mass range of  $m/z = 300$  to 2500,

with 1 s accumulation time. The source temperature was 350 °C and the spray voltage was set to 5500 V. Declustering potential value was set to 80 V. Peak View Software™ V.2.2 (version 2.2, Sciex, Redwood City, CA, USA) was used for deconvoluting the raw electrospray data to obtain the neutral molecular masses.

#### 4.5. Digestion and proteomics MS/MS analysis

After the labelling 40–50 µL of the sample and 10 µL 0.2% (w/v) RapiGest SF (Waters, Milford, USA) solution buffered with 50 mM ammonium bicarbonate were mixed (pH 7.8) and 3.3 µL of 45 mM DTT in 100 mM NH<sub>4</sub>HCO<sub>3</sub> were added and kept at 37.5 °C for 30 min. After cooling the sample to room temperature, 4.16 µL of 100 mM iodoacetamide in 100 mM NH<sub>4</sub>HCO<sub>3</sub> were added and placed in the dark in room temperature for 30 min. The reduced and alkylated protein was then digested by 10 µL (1 mg/mL) trypsin (the enzyme-to-protein ratio was 1:10) (Sigma, St Louis, MO, USA). The sample was incubated at 37 °C for overnight. To degrade the surfactant, 7 µL of formic acid (500 mM) solution was added to the digested protein sample to obtain the final 40 mM concentration (pH ≈ 2) and was incubated at 37 °C for 45 min. For LC-MS analysis, the acid treated sample was centrifuged for 5 min at 13 000 rpm. QTRAP 6500 triple quadrupole – linear ion trap mass spectrometer, equipped with a Turbo V source in electrospray mode (AB Sciex, CA, USA) and a PerkinElmer Series 200 micro LC system (Massachusetts, USA) was used for LC-MS/MS analysis. Data acquisition and processing were performed using Analyst software version 1.6.2 (AB Sciex Instruments, CA, USA). Chromatographic separation was achieved by using the Vydac 218 TP52 Protein & Peptide C18 column (250 mm × 2.1 mm, 5 µm). The sample was eluted with a gradient of solvent A (0.1% formic acid in water) and solvent B (0.1% formic acid in ACN). The flow rate was set to 0.2 mL/min. The initial conditions for separation were 5% B for 7 min, followed by a linear gradient to 90% B by 53 min, from 60 to 63 min 90% B is retained; from 64 to 65 min back to the initial conditions with 5% eluent B retained to 70 min. The injection volume was 10 µL (300 pmol on the column). Information Dependent Acquisition (IDA) LC-MS/MS experiment was used to identify the modified tryptic peptide fragments. Enhanced MS scan (EMS) was applied as survey scan and enhanced product ion (EPI) was the dependent scan. The collision energy in EPI experiments was set to rolling collision energy mode, where the actual value was set according to the mass and charge state of the selected ion. Further IDA criteria: ions greater than: 400.000 *m/z*, which exceeds 106 counts, exclude former target ions for 30 s after 2 occurrence(s). In EMS and in EPI mode the scan rate was 1000 Da/s as well. Nitrogen was used as the nebulizer gas (GS1), heater gas (GS2), and curtain gas with the optimum values set at 50, 40 and 40 (arbitrary units). The source temperature was 350 °C and the ion spray voltage set at 5000 V. Declustering potential value was set to 150 V. GPMW 4.2 software and ProteinProspector [61] was used to analyse the large number of MS-MS spectra and identify the modified tryptic peptides.

#### 4.6. NMR measurements of tau-K18

NMR measurements were performed as described earlier [21]. Briefly, protein and ligand-observed NMR data were obtained using Bruker AVANCE 600 MHz spectrometer (Bruker BioSpin, Fällanden, Switzerland) equipped with a BACS-120 sample changer and QCI-F cryoprobe in 50 mM NaP<sub>i</sub> pH 6.6, 25 mM NaCl, 100 µM DSS, 5% D<sub>2</sub>O, 4% DMSO-*d*<sub>6</sub> at 298 K, unless stated otherwise. Bruker DPX-400 spectrometer (Bruker BioSpin, Fällanden, Switzerland) was used to assess structural integrity of organic compounds in DMSO-*d*<sub>6</sub> at 298 K. The NMR data were processed and analyzed using TopSpin 4.0.2 (Bruker BioSpin, Fällanden, Switzerland), MNova 11.0

(MestreLab Research, Santiago de Compostela, Spain) and Dynamics Center 2.5.4 (Bruker BioSpin, Fällanden, Switzerland).

#### 4.7. tau-K18 aggregation protocol

We applied the same aggregation protocol for all assays to ensure comparability. Solutions of 10 µM tau K18 constructs in 25 mM pH 6.6 PBS (150 mM NaCl) were incubated undisturbed at 37 °C, in the presence of a 1:10 M ratio of heparin (MW 3000) as an initiator.

#### 4.8. Fluorescence assay of tau-K18 aggregation

The tau K18 constructs was incubated under standard aggregation conditions in the presence of 20 µM Thioflavin T in 96-well plates. The fluorescence intensity throughout incubation (37 °C for 24h) was monitored using a FLUOstar fluorescence plate reader. The ThT fluorescence was measured through the bottom of the plate approximately every 5 min, with excitation filter of 450 nm and emission filter of 486 nm. After 6 h the fluorescence intensity was maintained, then the time-binned data were used to calculate average level of aggregation compared to the non-aggregated negative control, and the non-treated but aggregated positive control.

#### 4.9. Circular dichroism (CD) spectroscopy

CD spectra were collected using a JASCO J-1500 spectropolarimeter at room temperature in a 0.1 cm path-length cylindrical quartz cuvette at a rate of 50 nm/min, with a data pitch of 0.5 nm, response time of 2 s, bandwidth of 2 nm, and 3 accumulations. Spectra were corrected by subtracting a blank and smoothed.

#### 4.10. Transmission electron microscopy (TEM)

For the transmission electron microscopic (TEM) studies Formvar/Carbon coated 300 mesh, copper grids (FCF300-CU, Formvar/Carbon 300 mesh, copper, electron Microscopy Sciences) were used. The process was carried out at RT on a sheet of parafilm placed in a Petri dish. 50 µL aliquots (drops) of each incubation solution were pipetted onto the parafilm in the following order: sample, distilled water, two drops of 1% uranyl-acetate, distilled water (DW). Using fine forceps, the grid was placed onto the drop of sample for 1 min. After blotting off excess liquid with filter paper the grid was briefly rinsed on the first drop of DW then on the first drop of uranyl-acetate. Next, the grid was placed onto the second drop of uranyl-acetate for 1 min and finally for a short rinse on the second drop of DW. Between each step, excess liquid was blotted by filter paper. The grids were investigated with a JEOL TEM-1011 (JEOL, Tokyo, Japan) equipped with a Mega-View-III digital camera. For a detailed description, see relevant literature [62]. Semi-quantitative analysis was performed by ImageJ® software as follows. First background subtraction was performed applying a sliding paraboloid algorithm with 30.0 pixels rolling ball radius, then weighted average brightness of the images was calculated based on the pixel intensity histogram analysis. Results are given as average of 5 parallel micrograph evaluation.

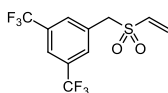
#### 4.11. Synthetic procedures

##### 4.11.1. General procedure for vinylsulfone synthesis [63]

The appropriate halogen derivative (bromine for **11**, **28**, **30**, **31** and chlorine for **29**) (5 mmol) was dissolved in *N,N*-dimethylformamide (10 mL) and added dropwise to the solution of

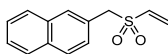
2-mercaptoethanol (350  $\mu\text{L}$ , 5 mmol) and potassium carbonate (1037 mg, 7.5 mmol) in *N,N*-dimethylformamide (20 mL), then the mixture was stirred at RT. After 3 h, the solvent was evaporated and the residue was dissolved in 50 mL ethyl acetate, then washed with 50 mL brine. The organic layer was dried and concentrated. The crude product was dissolved in 50 mL dichloromethane and meta-chloroperoxybenzoic acid (2.16 g, 12.5 mmol) was added slowly. The mixture was stirred for 3 h, and then washed with 1 M aqueous solution of sodium hydroxide. After the extraction, the organic phase was dried and concentrated, then the product was dissolved in 20 mL dry dichloromethane. To this solution, methanesulfonylchloride (464  $\mu\text{L}$ , 6 mmol) was added at 0  $^{\circ}\text{C}$ , and triethylamine (1043  $\mu\text{L}$ , 7.5 mmol) was dropped slowly into the mixture. After the addition of the base, the reaction mixture was heated up to RT and stirred for 2 h. Finally, the solvent was removed, and crude product was purified by column chromatography with hexane and ethylacetate as eluents.

#### 4.11.2. 1,3-Bis(trifluoromethyl)-5-((vinylsulfonyl)methyl)benzene (**11**) [43]



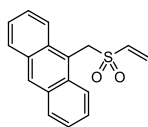
Yield: 21% (328 mg).  $^1\text{H}$  NMR (500 MHz,  $\text{DMSO}-d_6$ ):  $\delta$  8.14 (s, 1H), 8.09 (s, 2H), 7.00 (dd,  $J = 16.6, 10.0$  Hz, 1H), 6.26 (d,  $J = 9.9$  Hz, 1H), 6.08 (d,  $J = 16.6$  Hz, 1H), 4.84 (s, 2H) ppm.  $^{13}\text{C}$  NMR (125 MHz,  $\text{CDCl}_3$ ):  $\delta$  136.4, 132.8, 132.2 (2C), 131.8, 130.7 (q,  $J = 32.5$  Hz, 2C), 123.6 (q,  $J = 271.3$  Hz, 2C), 122.8–122.6 (m), 57.9 ppm [43]. Mp. 72  $^{\circ}\text{C}$ . HRMS (DUIS): (M – H) $^-$  calcd. for  $\text{C}_{11}\text{H}_7\text{F}_6\text{O}_2\text{S}^-$ , 317.0076; found 317.0046.

#### 4.11.3. 2-((Vinylsulfonyl)methyl)naphthalene (**28**)



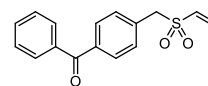
Yield: 27% (313 mg).  $^1\text{H}$  NMR (500 MHz,  $\text{CDCl}_3$ ):  $\delta$  7.88–7.83 (m, 4H), 7.55–7.48 (m, 3H), 6.54 (dd,  $J = 16.6, 9.9$  Hz, 1H), 6.30 (d,  $J = 16.6$  Hz, 1H), 6.07 (d,  $J = 9.9$  Hz, 1H), 4.42 (s, 2H) ppm.  $^{13}\text{C}$  NMR (125 MHz,  $\text{CDCl}_3$ ):  $\delta$  135.3, 133.3, 133.2, 131.2, 130.5, 128.7, 128.0, 127.8, 127.7, 126.8, 126.6, 125.1, 61.2 ppm. Mp. 195–196  $^{\circ}\text{C}$ . HRMS (DUIS): (M + H) $^+$  calcd. for  $\text{C}_{13}\text{H}_{13}\text{O}_2\text{S}^+$ , 233.0636; found, 233.0659.

#### 4.11.4. 9-((Vinylsulfonyl)methyl)anthracene (**29**)



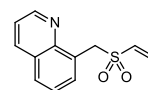
Yield: 19% (268 mg).  $^1\text{H}$  NMR (500 MHz,  $\text{CDCl}_3$ ):  $\delta$  8.55 (s, 1H), 8.29 (d,  $J = 9.0$  Hz, 2H), 8.06 (d,  $J = 8.4$  Hz, 2H), 7.66–7.58 (m, 2H), 7.56–7.48 (m, 2H), 6.48 (dd,  $J = 16.5, 9.8$  Hz, 1H), 6.32 (d,  $J = 16.6$  Hz, 1H), 5.91 (d,  $J = 9.8$  Hz, 1H), 5.43 (s, 2H) ppm.  $^{13}\text{C}$  NMR (125 MHz,  $\text{CDCl}_3$ ):  $\delta$  135.4, 131.9, 130.9, 130.2, 128.7, 126.3, 125.4, 125.2, 124.3, 122.1, 58.1 ppm. Mp. 221–224  $^{\circ}\text{C}$ . HRMS (DUIS): (M + H) $^+$  calcd. for  $\text{C}_{17}\text{H}_{15}\text{O}_2\text{S}^+$ , 283.0787; found, 283.0776.

#### 4.11.5. Phenyl(4-((vinylsulfonyl)methyl)phenyl)methanone (**30**)



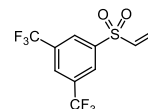
Yield: 31% (443 mg).  $^1\text{H}$  NMR (500 MHz,  $\text{CDCl}_3$ ):  $\delta$  7.83–7.78 (m, 4H), 7.66–7.64 (m, 1H), 7.54–7.36 (m, 4H), 6.82 (dd,  $J = 16.5, 10.0$  Hz, 1H), 6.39 (d,  $J = 16.5$  Hz, 1H), 6.01 (d,  $J = 9.9$  Hz, 1H), 4.73 (s, 2H) ppm.  $^{13}\text{C}$  NMR (125 MHz,  $\text{CDCl}_3$ ):  $\delta$  195.4, 140.8, 137.3, 136.8, 135.2, 132.6, 130.6, 130.1, 129.2, 128.4, 122.1, 61.9 ppm. Mp. 179  $^{\circ}\text{C}$ . HRMS (DUIS): (M + H) $^+$  calcd. for  $\text{C}_{16}\text{H}_{15}\text{O}_3\text{S}^+$ , 287.0736; found, 287.0719.

#### 4.11.6. 8-((Vinylsulfonyl)methyl)quinoline (**31**)



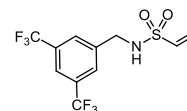
Yield: 12% (140 mg).  $^1\text{H}$  NMR (500 MHz,  $\text{CDCl}_3$ ):  $\delta$  8.01 (dd,  $J = 4.2, 1.8$  Hz, 1H), 8.17 (dd,  $J = 8.3, 1.9$  Hz, 1H), 7.85 (dd,  $J = 7.1, 1.4$  Hz, 1H), 7.80 (dd,  $J = 8.2, 1.4$  Hz, 1H), 7.52 (t,  $J = 7.5$ , 1H), 7.45 (dd,  $J = 8.3, 4.1$  Hz, 1H), 6.90 (dd,  $J = 16.5, 9.9$  Hz, 1H), 6.33 (d,  $J = 16.6$  Hz, 1H), 6.12 (d,  $J = 9.9$  Hz, 1H), 4.89 (s, 2H) ppm.  $^{13}\text{C}$  NMR (125 MHz,  $\text{CDCl}_3$ ):  $\delta$  156.9, 146.5, 130.3, 127.9, 127.5, 125.4, 122.3, 121.3, 59.8 ppm. Mp. 142  $^{\circ}\text{C}$ . HRMS (DUIS): (M + H) $^+$  calcd. for  $\text{C}_{12}\text{H}_{12}\text{O}_2\text{NS}^+$ , 234.0589; found, 224.0568.

#### 4.11.7. 3,5-Bis(trifluoromethyl)phenyl vinylsulfone (**32**) [43]



Synthetic procedure was performed as described in literature [43]. Yield: 14% (128 mg).  $^1\text{H}$  NMR (500 MHz,  $\text{DMSO}-d_6$ ):  $\delta$  8.34 (s, 2H), 8.13 (s, 1H), 6.74–6.61 (m, 2H), 6.24 (d,  $J = 8.7$  Hz, 1H) ppm.  $^{13}\text{C}$  NMR (125 MHz,  $\text{CDCl}_3$ ):  $\delta$  135.9, 132.6, 132.1 (2C), 131.9, 131.0 (q,  $J = 32.4$  Hz, 2C), 123.8 (q,  $J = 271.4$  Hz, 2C), 122.9–122.5 (m), 58.2 ppm [64]. Mp. 46–48  $^{\circ}\text{C}$ .

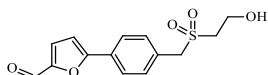
#### 4.11.8. *N*-(3,5-Bis(trifluoromethyl)benzyl)ethenesulfonamide (**33**) [43]



Synthetic procedure was performed as described in literature [43]. Yield: 53% (882 mg).  $^1\text{H}$  NMR (500 MHz,  $\text{DMSO}-d_6$ ):  $\delta$  8.04 (t,  $J = 6.3$  Hz, 1H), 8.03 (s, 2H), 8.00 (s, 1H), 6.74 (dd,  $J = 16.5, 10.0$  Hz, 1H), 6.06 (d,  $J = 16.5$  Hz, 1H), 5.98 (d,  $J = 10.0$  Hz, 1H), 4.28 (d,  $J = 6.3$  Hz, 2H) ppm.  $^{13}\text{C}$  NMR (125 MHz,  $\text{DMSO}-d_6$ ):  $\delta$  147.3, 142.0, 135.4 (q,  $J = 32.5$  Hz, 2C), 133.6 (2C), 131.2, 128.5 (q,  $J = 271.3$  Hz, 2C), 126.3–126.0 (m), 49.9 ppm [43]. Mp. 55  $^{\circ}\text{C}$ . HRMS (DUIS): (M – H) $^-$  calcd. for  $\text{C}_{11}\text{H}_8\text{F}_6\text{NO}_2\text{S}^-$ , 332.0185; found 332.0157.

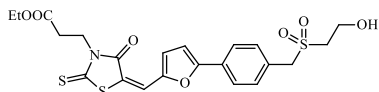
## 4.12. Synthesis of rhodanine derivative

### 4.12.1. 5-(4-(((2-hydroxyethyl)sulfonyl)methyl)phenyl)furan-2-carbaldehyde



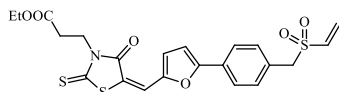
In a sealed tube 2-((4-bromobenzyl)sulfonyl)ethan-1-ol (307 mg, 1.1 mmol), (5-formylfuran-2-yl)boronic acid (154 mg, 1.1 mmol), potassium carbonate (304 mg, 2.0 mmol, 1.9 equiv.) and tetrakis(triphenylphosphino)palladium(0) (127 mg, 0.11 mmol, 10%) was mixed in 20 mL toluene:EtOH 7:3, and heated at 100 °C for 4 h. The solvent was evaporated and divided between 20 mL EtOAc and 20 mL water. After the separation, the organic phase was evaporated to silica, and the crude product was purified by flash column chromatography resulting in a mixture containing the product that could not be separated from cross-coupling side products. The 180 mg (80% purity) was taken to the next reaction step.

### 4.12.2. Ethyl (E)-3-(5-(((5-(4-(((2-hydroxyethyl)sulfonyl)methyl)phenyl)furan-2-yl)methylene)-4-oxo-2-thioxothiazolidin-3-yl)propanoate



In a round bottom flask 5-(((5-(4-(((2-hydroxyethyl)sulfonyl)methyl)phenyl)furan-2-yl)methylene)-4-oxo-2-thioxothiazolidin-3-yl)propanoate (70 mg, 0.3 mmol) and piperidine (60  $\mu$ L, 0.6 mmol, 2 equiv.) was added, and the reaction mixture was stirred at RT overnight. After evaporation to silica, the crude product was purified by flash column chromatography resulting in the product as a white solid (60 mg, 39%). <sup>1</sup>H NMR (500 MHz, DMSO-*d*<sub>6</sub>)  $\delta$  7.88 (d, *J* = 8.3 Hz, 2H), 7.71 (s, 1H), 7.59 (d, *J* = 8.2 Hz, 2H), 7.39 (d, *J* = 3.8 Hz, 1H), 7.37 (d, *J* = 3.8 Hz, 1H), 5.74 (s, 4H), 5.22 (t, *J* = 5.2 Hz, 1H), 4.55 (s, 2H), 4.28 (t, *J* = 7.4 Hz, 2H), 4.05 (q, *J* = 7.1 Hz, 2H), 3.84 (q, *J* = 5.6 Hz, 2H), 3.19 (t, *J* = 5.9 Hz, 2H), 2.71 (t, *J* = 7.6 Hz, 2H), 1.17 (t, *J* = 7.1 Hz, 3H) ppm; <sup>13</sup>C NMR (126 MHz, DMSO-*d*<sub>6</sub>)  $\delta$  170.6, 160.1, 158.1, 149.9, 132.6, 130.3, 128.9, 124.9, 123.6, 119.2, 118.9, 111.2, 60.8, 60.0, 55.4, 55.3, 54.6, 43.5, 31.5, 14.4 ppm. Mp. 123–124 °C. HRMS (DUIS): (M + H)<sup>+</sup> calcd. for C<sub>22</sub>H<sub>24</sub>O<sub>7</sub>NS<sub>3</sub><sup>+</sup>, 510.0715; found, 510.0694.

### 4.12.3. Ethyl (E)-3-(4-oxo-2-thioxo-5-(((5-(4-(((vinylsulfonyl)methyl)phenyl)furan-2-yl)methylene)thiazolidin-3-yl)propanoate (34)

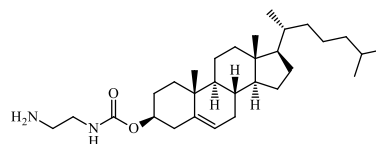


In a round bottom flask ethyl (E)-3-(5-(((5-(4-(((2-hydroxyethyl)sulfonyl)methyl)phenyl)furan-2-yl)methylene)-4-oxo-2-thioxothiazolidin-3-yl)propanoate (41 mg, 0.08 mmol) was dissolved in 30 mL dichloromethane followed by methanesulfonyl chloride (9  $\mu$ L, 0.12 mmol, 1.5 equiv.) and diisopropyl ethylamine (122  $\mu$ L, 0.89 mmol, 11 equiv.) at 0 °C. The reaction mixture was

stirred overnight at RT. The solution was washed by 2 x 30 mL water, then dried (MgSO<sub>4</sub>), and the solvent was evaporated resulting the product as a white solid (13 mg, 33%). <sup>1</sup>H NMR (500 MHz, CDCl<sub>3</sub>)  $\delta$  7.81 (d, *J* = 8.2 Hz, 1H), 7.54–7.45 (m, 2H), 6.98 (d, *J* = 3.7 Hz, 1H), 6.91 (t, *J* = 4.5 Hz, 1H), 6.60–6.49 (m, 1H), 6.38–6.30 (m, 1H), 6.19–6.12 (m, 1H), 4.46 (t, *J* = 7.5 Hz, 1H), 4.30 (s, 2H), 4.20–4.11 (m, 2H), 2.78 (t, *J* = 7.6 Hz, 1H), 2.06 (s, 2H), 1.32–1.24 (m, 5H) ppm; <sup>13</sup>C NMR (126 MHz, CDCl<sub>3</sub>)  $\delta$  209.9, 202.4, 200.2, 175.0, 157.4, 149.4, 143.6, 131.2, 124.6, 111.8, 109.3, 104.0, 101.1, 82.0, 60.5, 39.6, 31.0, 13.7 ppm. Mp. 158 °C. HRMS (DUIS): (M + H)<sup>+</sup> calcd. for C<sub>22</sub>H<sub>22</sub>O<sub>6</sub>NS<sub>3</sub><sup>+</sup>, 492.0609; found, 492.0642.

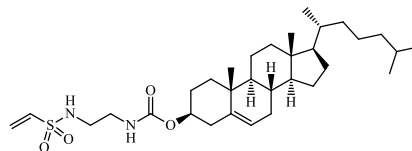
## 4.13. Synthesis of cholesterol derivatives

### 4.13.1. 3 $\beta$ -Cholest-5-en-3-yl (2-aminoethyl)carbamate



In a round bottom flask triethylamine (3 mmol, 0.52 mL, 3 equiv.) and 1,2-ethylenediamine (20 mmol, 1.34 mL, 20 equiv.) was dissolved in 90 mL dichloromethane. 3 $\beta$ -Cholest-5-en-3-yl chloroformate (1 mmol, 0.5 g) was slowly added in 10 mL dichloromethane at 0 °C. The reaction mixture was stirred at room temperature overnight, then washed with 2 x 30 mL water. The organic phase was dried over MgSO<sub>4</sub>, and the solvent was evaporated in vacuo. The product (370 mg, 78%) was used without further purification as a white solid. <sup>1</sup>H NMR (CDCl<sub>3</sub>, 500 MHz)  $\delta$  5.41–5.36 (m, 1H), 4.95 (s, 1H), 4.56–4.47 (m, 1H), 3.23 (dd, *J* = 11.5, 5.7 Hz, 2H), 2.83 (t, *J* = 5.9 Hz, 2H), 2.41–2.34 (m, 1H), 2.29 (t, *J* = 11.2 Hz, 1H), 2.05–1.94 (m, 2H), 1.94–1.79 (m, 3H), 1.62–1.05 (m, 22H), 1.02 (s, 4H), 1.00–0.95 (m, 3H), 0.93 (d, *J* = 6.5 Hz, 3H), 0.88 (dd, *J* = 6.6, 2.2 Hz, 6H) ppm; <sup>13</sup>C NMR (126 MHz, CDCl<sub>3</sub>)  $\delta$  156.5, 139.8, 122.5, 74.5, 56.7, 56.2, 50.0, 42.5, 42.3, 41.4, 39.8, 39.5, 38.6, 37.0, 36.6, 36.2, 35.8, 31.9, 28.2, 28.1, 28.0, 24.3, 23.9, 22.8, 22.5, 21.1, 19.3, 18.7, 11.9 ppm. Mp. 147–149 °C. HRMS (DUIS): (M + H)<sup>+</sup> calcd. for C<sub>30</sub>H<sub>53</sub>O<sub>2</sub>N<sub>2</sub><sup>+</sup>, 473.4107; found, 473.4078.

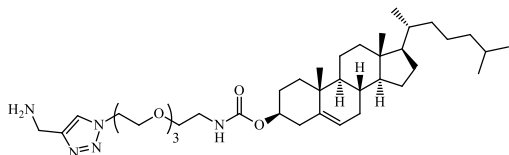
### 4.13.2. 3 $\beta$ -Cholest-5-en-3-yl (2-(vinylsulfonylamido)ethyl)carbamate (35)



In a round bottom flask 3 $\beta$ -cholest-5-en-3-yl (2-aminoethyl) carbamate (0.22 mmol, 104 mg) and triethylamine (0.44 mmol, 61  $\mu$ L, 2 equiv.) was dissolved in 10 mL dichloromethane followed by the addition of chloroethanesulfonyl chloride (0.44 mmol, 46  $\mu$ L, 2 equiv.) at 0 °C. After 1 h triethylamine (0.44 mmol, 61  $\mu$ L, 2 equiv.) was added, and the reaction mixture was stirred at RT overnight. The reaction mixture was washed with 10 mL water, 10 mL brine and 10 mL 10% HCl solution, then dried over MgSO<sub>4</sub>. The solvent was evaporated in vacuo to gain the product as a colourless film (110 mg, 89%). <sup>1</sup>H NMR (500 MHz, CDCl<sub>3</sub>)  $\delta$  6.59–6.50 (m, 1H), 6.42 (d, *J* = 16.7 Hz, 1H), 6.26 (d, *J* = 16.6 Hz, 1H), 6.12 (d, *J* = 9.9 Hz, 1H), 5.95 (d, *J* = 9.8 Hz, 1H), 5.38 (s, 1H), 5.02 (s, 1H), 4.50 (s, 1H), 4.22 (q,

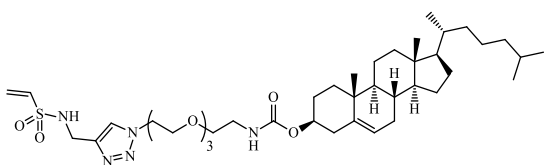
$J = 6.8$  Hz, 1H), 3.38–3.27 (m, 1H), 3.18 (d,  $J = 3.9$  Hz, 1H), 2.40–2.25 (m, 2H), 2.00 (t,  $J = 17.9$  Hz, 2H), 1.93–1.79 (m, 3H), 1.63–1.44 (m, 6H), 1.41 (t,  $J = 7.1$  Hz, 3H), 1.38–1.05 (m, 10H), 1.02 (s, 4H), 0.93 (d,  $J = 6.0$  Hz, 3H), 0.88 (d,  $J = 6.4$  Hz, 5H), 0.69 (s, 3H) ppm.  $^{13}\text{C}$  NMR (126 MHz,  $\text{CDCl}_3$ )  $\delta$  156.8, 139.6, 135.9, 126.7, 122.7, 74.9, 56.7, 56.2, 50.0, 43.4, 42.3, 40.9, 39.7, 39.5, 38.5, 37.0, 36.6, 36.2, 35.8, 31.9, 28.2, 28.1, 28.0, 24.3, 23.8, 22.8, 22.5, 21.0, 19.3, 18.7, 11.8 ppm. Mp. 192–195 °C. HRMS (DUIS):  $(\text{M} + \text{H})^+$  calcd. for  $\text{C}_{32}\text{H}_{55}\text{O}_4\text{N}_2\text{S}^+$ , 563.3883; found, 563.3907.

#### 4.13.3. $\beta$ -Cholest-5-en-3-yl (2-(2-(2-(2-(4-(aminomethyl)-1H-1,2,3-triazol-1-yl)ethoxy)ethoxy)ethoxy)ethyl)carbamate



$\beta$ -Cholest-5-en-3-yl (2-(2-(2-(2-azidoethoxy)ethoxy)ethoxy)ethyl)carbamate (35 mg, 0.06 mmol) was dissolved in 3 mL  $\text{DMSO}:\text{H}_2\text{O}$  1:1, then propargylamine (8  $\mu\text{L}$ , 0.12 mmol, 2 equiv.),  $\text{CuI}$  (8 mg, 0.04 mmol, 0.7 equiv.) and THPTA (22 mg, 0.05 mmol, 0.85 equiv.) was added. The reaction mixture was stirred at RT overnight. The next day the same amount of alkyne and catalysts were added, stirred at 37 °C for 4 h then RT overnight. 10 mL water was added, and the aqueous solution was extracted with  $\text{EtOAc}$  (3 x 10 mL). The organic phase was dried ( $\text{MgSO}_4$ ), filtered, and evaporated resulting in a white solid (22 mg, 63%).  $^1\text{H}$  NMR (500 MHz,  $\text{CDCl}_3$ )  $\delta$  5.37 (s, 1H), 5.31–5.24 (m, 1H), 4.60–4.56 (m, 1H), 4.56–4.53 (m, 1H), 4.53–4.45 (m, 1H), 3.89 (q,  $J = 5.0$  Hz, 1H), 3.75 (t,  $J = 6.5$  Hz, 2H), 3.64–3.59 (m, 5H), 3.58 (d,  $J = 3.5$  Hz, 3H), 3.57–3.51 (m, 2H), 3.39–3.32 (m, 2H), 2.38–2.31 (m, 1H), 2.30–2.20 (m, 1H), 2.03–1.93 (m, 2H), 1.89–1.79 (m, 4H), 1.61–1.44 (m, 6H), 1.43 (s, 1H), 1.41–1.28 (m, 4H), 1.29–1.21 (m, 3H), 1.20–1.03 (m, 8H), 1.00 (s,  $J = 11.1$  Hz, 4H), 0.97–0.93 (m, 1H), 0.91 (d,  $J = 6.5$  Hz, 3H), 0.87 (dd,  $J = 6.6, 2.2$  Hz, 7H) ppm.  $^{13}\text{C}$  NMR (126 MHz,  $\text{CDCl}_3$ )  $\delta$  156.8, 139.8, 129.9, 123.1, 122.3, 77.3, 70.4, 70.3, 56.7, 56.0, 50.0, 42.7, 39.7, 39.5, 38.8, 37.9, 37.0, 36.7, 36.2, 35.8, 31.9, 29.7, 28.1, 28.0, 24.3, 23.8, 22.8, 25.5, 21.1, 19.3, 18.7, 11.9 ppm. Mp. 141–143 °C. HRMS (DUIS):  $(\text{M} + \text{H})^+$  calcd. for  $\text{C}_{35}\text{H}_{60}\text{O}_3\text{N}_5$ , 598.4696; found, 598.4680.

#### 4.13.4. $\beta$ -Cholest-5-en-3-yl (2-(2-(2-(2-(4-(vinylsulfonylamidomethyl)-1H-1,2,3-triazol-1-yl)ethoxy)ethoxy)ethoxy)ethyl)carbamate (36)



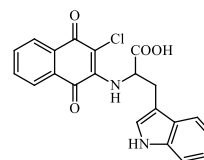
In a round bottom flask  $\beta$ -Cholest-5-en-3-yl (2-(2-(2-(2-(4-(aminomethyl)-1H-1,2,3-triazol-1-yl)ethoxy)ethoxy)ethoxy)ethyl)carbamate (105 mg, 0.22 mmol) and triethylamine (30  $\mu\text{L}$ , 0.22 mmol, 1 equiv.) was dissolved in 10 mL dichloromethane. 2-Chloroethanesulfonyl chloride (23  $\mu\text{L}$ , 0.22 mmol, 1 equiv.) was added at 0 °C, and after 1 h triethylamine (30  $\mu\text{L}$ , 0.22 mmol, 1 equiv.) was added again. The reaction mixture was stirred at RT overnight. To reach full conversion, the addition of the amine (2

equiv.) and the sulfonyl chloride (1 equiv.) was repeated. The solution was washed with 10 mL water, 10 mL brine and 10 mL 10%  $\text{HCl}$  before drying ( $\text{MgSO}_4$ ) and evaporating the organic solvent in vacuo resulting in a colourless film (110 mg, 89%).  $^1\text{H}$  NMR (500 MHz,  $\text{CDCl}_3$ )  $\delta$  6.59–6.50 (m, 1H), 6.42 (d,  $J = 16.7$  Hz, 1H), 6.26 (d,  $J = 16.6$  Hz, 1H), 6.12 (d,  $J = 9.9$  Hz, 1H), 5.95 (d,  $J = 9.8$  Hz, 1H), 5.38 (s, 1H), 5.02 (s, 1H), 4.50 (s, 1H), 4.22 (q,  $J = 6.8$  Hz, 1H), 3.38–3.27 (m, 1H), 3.18 (d,  $J = 3.9$  Hz, 1H), 2.40–2.25 (m, 2H), 2.00 (t,  $J = 17.9$  Hz, 2H), 1.93–1.79 (m, 3H), 1.63–1.44 (m, 6H), 1.41 (t,  $J = 7.1$  Hz, 3H), 1.38–1.05 (m, 10H), 1.02 (s, 4H), 0.93 (d,  $J = 6.0$  Hz, 3H), 0.88 (d,  $J = 6.4$  Hz, 5H), 0.69 (s, 3H) ppm.  $^{13}\text{C}$  NMR (126 MHz,  $\text{CDCl}_3$ )  $\delta$  157.6, 147.7, 139.8, 129.7, 123.1, 122.5, 117.2, 77.3, 70.4, 70.3, 56.7, 56.1, 50.0, 42.3, 39.7, 39.5, 38.6, 37.9, 37.0, 36.6, 36.2, 35.8, 31.9, 29.7, 28.2, 28.0, 24.3, 23.8, 22.8, 25.5, 21.0, 19.3, 18.7, 11.8 ppm. Mp. 184–187 °C. HRMS (DUIS):  $(\text{M} + \text{H})^+$  calcd. for  $\text{C}_{37}\text{H}_{62}\text{O}_5\text{N}_5\text{S}^+$ , 688.4472; found, 688.4413.

## 5. Synthesis of W-MINK-derivative

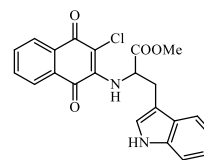
### 5.1. Synthesis of peptide modifiers (Cl-NQTrp head and vinylsulfone warhead tail)

#### 5.1.1. (3-chloro-1,4-dioxo-1,4-dihydronaphthalen-2-yl)tryptophan



In a round bottom flask 2,3-dichloronaphthalene-1,4-dione (4.5 g, 20 mmol) was dissolved in 400 mL  $\text{MeOH}$ , and then tryptophan (4.1 g, 20 mmol) was added in aqueous  $\text{KOH}$  (5 mL/mmol, 2.2 g, 40 mmol, 2 equiv.) solution. The reaction mixture was stirred at RT overnight, then 500 mL 10%  $\text{HCl}$  solution was added slowly. The precipitated salt was filtered, and washed with water, then purified by flash column chromatography resulting in the product as a dark red solid (4.3 g, 54%).  $^1\text{H}$  NMR (500 MHz,  $\text{DMSO}-d_6$ )  $\delta$  13.27 (s, 1H), 10.95 (s, 1H), 7.95 (d,  $J = 7.5$  Hz, 1H), 7.88 (d,  $J = 6.0$  Hz, 1H), 7.82 (t,  $J = 7.4$  Hz, 1H), 7.73 (t,  $J = 7.4$  Hz, 1H), 7.51 (d,  $J = 7.9$  Hz, 1H), 7.30 (d,  $J = 8.0$  Hz, 1H), 7.22 (s, 1H), 7.04 (t,  $J = 7.4$  Hz, 1H), 6.94 (t,  $J = 7.3$  Hz, 1H), 6.60 (s, 1H), 5.35 (d,  $J = 6.2$  Hz, 1H), 3.41 (t,  $J = 5.2$  Hz, 2H). APT NMR (125 MHz,  $\text{DMSO}-d_6$ )  $\delta$  173.1, 136.6, 134.9, 134.1, 132.1, 130.4, 129.1, 128.2, 127.8, 127.0, 126.2, 126.0, 125.1, 121.9, 118.6, 118.1, 111.9, 108.3, 57.1, 29.1 ppm. Mp 150 °C (lit. 148–150 °C) [65]. HRMS (DUIS):  $(\text{M} + \text{H})^+$  calcd. for  $\text{C}_{21}\text{H}_{16}\text{O}_4\text{N}_2\text{Cl}^+$ , 395.0793; found, 395.0788.

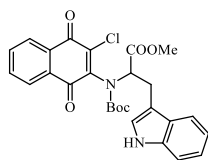
#### 5.1.2. Methyl (3-chloro-1,4-dioxo-1,4-dihydronaphthalen-2-yl)tryptophanate



In a round bottom flask 3-chloro-1,4-dioxo-1,4-dihydronaphthalen-2-yl)tryptophan (2.6 g, 6.6 mmol) was suspended in 250 mL methanol at 0 °C, and thionyl chloride (2.5 mL, 1.5 g, 12.6 mmol, 1.9 equiv.) was added dropwise. The reaction mixture was stirred at RT overnight, then the solvent was

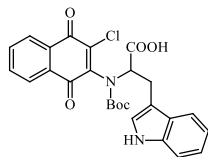
evaporated resulting in the product as a red solid (2.5 g, 93%).  $^1\text{H}$  NMR (500 MHz,  $\text{DMSO-}d_6$ )  $\delta$  10.98 (s, 1H), 7.93 (d,  $J = 7.5$  Hz, 1H), 7.87 (d,  $J = 7.5$  Hz, 1H), 7.79 (t,  $J = 7.5$  Hz, 1H), 7.71 (t,  $J = 7.5$  Hz, 1H), 7.45 (d,  $J = 7.9$  Hz, 1H), 7.31 (d,  $J = 8.1$  Hz, 1H), 7.25 (d,  $J = 2.1$  Hz, 1H), 7.04 (t,  $J = 7.5$  Hz, 1H), 6.96 (t,  $J = 7.4$  Hz, 1H), 6.60 (s, 1H), 5.38 (d,  $J = 6.3$  Hz, 1H), 3.69 (s, 4H), 3.39 (d,  $J = 5.0$  Hz, 2H) ppm; APT NMR (125 MHz,  $\text{DMSO-}d_6$ )  $\delta$  172.2, 136.7, 135.4, 133.4, 131.9, 130.2, 129.3, 128.6, 127.5, 127.0, 126.3, 125.8, 125.1, 121.7, 119.1, 118.4, 112.0, 108.2, 57.2, 52.9, 29.0 ppm. Mp. 81 °C. HRMS (DUIS):  $(\text{M} + \text{H})^+$  calcd. for  $\text{C}_{22}\text{H}_{18}\text{O}_4\text{N}_2\text{Cl}^+$ , 409.0949; found, 409.0932.

### 5.1.3. Methyl $\text{N}^\alpha$ -(*tert*-butoxycarbonyl)- $\text{N}^\beta$ -(3-chloro-1,4-dioxo-1,4-dihydronaphthalen-2-yl)tryptophanate



In a round bottom flask methyl (3-chloro-1,4-dioxo-1,4-dihydronaphthalen-2-yl)tryptophanate (2.4 g, 5.9 mmol), di-(*tert*-butyl)-carbonate (3.2 g, 14.6 mmol, 2.5 equiv.), 4-dimethylaminopyridine (220 mg, 1.8 mmol, 30%) and triethylamine (2 mL, 2.74 g, 27.1 mmol, 4.6 equiv.) was added to 150 mL acetonitrile and stirred at RT for 1 h. The solvent was evaporated, and the crude product was purified by flash column chromatography resulting in the product as a red foam (1.4 g, 47%).  $^1\text{H}$  NMR (500 MHz,  $\text{DMSO-}d_6$ )  $\delta$  7.94–7.90 (m, 2H), 7.79 (t,  $J = 7.0$  Hz, 2H), 7.72–7.68 (m, 1H), 7.57–7.54 (m, 2H), 7.30–7.18 (m, 2H), 6.83 (d,  $J = 7.9$  Hz, 1H), 5.42 (dd,  $J = 12.9, 7.7$  Hz, 1H), 3.70 (s, 3H), 3.38 (t,  $J = 7.1$  Hz, 2H), 1.56 (s, 9H) ppm; APT NMR (125 MHz,  $\text{DMSO-}d_6$ )  $\delta$  182.3, 175.8, 171.9, 149.2, 135.5, 135.3, 135.1, 133.4, 131.7, 130.4, 130.3, 126.9, 126.2, 125.4, 124.9, 123.1, 119.4, 115.5, 115.1, 84.1, 56.8, 52.9, 28.3, 28.1 ppm. Mp. 80 °C. HRMS (DUIS):  $(\text{M} + \text{H})^+$  calcd. for  $\text{C}_{27}\text{H}_{26}\text{O}_6\text{N}_2\text{Cl}^+$ , 509.1473; found, 509.1454.

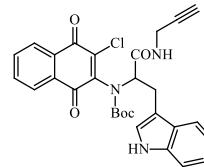
### 5.1.4. $\text{N}^\alpha$ -(*Tert*-butoxycarbonyl)- $\text{N}^\beta$ -(3-chloro-1,4-dioxo-1,4-dihydronaphthalen-2-yl)tryptophan



In a round bottom flask methyl  $\text{N}^\alpha$ -(*tert*-butoxycarbonyl)- $\text{N}^\beta$ -(3-chloro-1,4-dioxo-1,4-dihydronaphthalen-2-yl)tryptophanate (170 mg, 0.33 mmol) was dissolved in 20 mL tetrahydrofuran, and LiOH hydrate (42 mg, 1 mmol, 3 equiv.) was added. The reaction mixture was stirred at RT for 5 days, then the solvent was evaporated. 10 mL 1 M acetic acid was added with 20 mL dichloromethane and 2 mL MeOH. The organic phase was dried ( $\text{MgSO}_4$ ) and evaporated in vacuo resulting in the product as a dark brown oil (139 mg, 85%).  $^1\text{H}$  NMR (500 MHz,  $\text{DMSO-}d_6$ )  $\delta$  7.95–7.73 (m, 4H), 7.64 (s, 1H), 7.51 (s, 2H), 7.27 (s, 1H), 7.18 (s, 1H), 7.06 (s, 1H), 5.00 (s, 1H), 3.17 (s, 2H), 1.48 (s, 9H) ppm; APT NMR (125 MHz,  $\text{DMSO-}d_6$ )  $\delta$  183.5, 175.6, 170.0, 147.5, 135.3, 133.1, 132.9, 126.7, 126.3, 125.3, 124.5, 122.7, 119.9, 114.9, 110.0, 83.7, 60.2, 28.0 ppm. Mp.

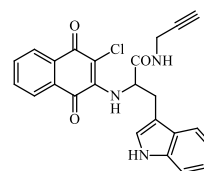
159–160 °C. HRMS (DUIS):  $(\text{M} + \text{H})^+$  calcd. for  $\text{C}_{26}\text{H}_{24}\text{O}_6\text{N}_2\text{Cl}^+$ , 495.1323; found, 495.1376.

### 5.1.5. *Tert*-butyl (3-(1*H*-indol-3-yl)-1-oxo-1-(prop-2-yn-1-ylamino)propan-2-yl)(3-chloro-1,4-dioxo-1,4-dihydronaphthalen-2-yl)carbamate



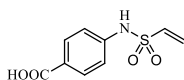
2-Propyn-1-amine (18  $\mu\text{L}$ , 0.29 mmol, 1.6 equiv.) was added to an ice bath cooled solution of  $\text{N}^\alpha$ -(*tert*-butoxycarbonyl)- $\text{N}^\beta$ -(3-chloro-1,4-dioxo-1,4-dihydronaphthalen-2-yl)tryptophan (89 mg, 0.18 mmol) in 10 mL dichloromethane. Anhydrous HOBt (23 mg, 0.17 mmol, 95%) and *N*-(3-dimethylaminopropyl)-*N'*-ethylcarbodiimide hydrochloride (35 mg, 0.18 mmol) were added at RT. The reaction mixture was stirred for 90 min, then the solvent was evaporated, and the crude product was purified by flash column chromatography resulting in the product as a red solid (88 mg, 92%).  $^1\text{H}$  NMR (300 MHz,  $\text{DMSO-}d_6$ )  $\delta$  8.94 (s, 1H), 7.97–7.75 (m, 3H), 7.75–7.59 (m, 3H), 7.42 (s, 1H), 7.32–7.17 (m, 2H), 6.77 (s, 1H), 5.41 (dd,  $J = 13.6, 6.9$  Hz, 1H), 3.94 (s, 2H), 3.22 (d,  $J = 22.4$  Hz, 2H), 3.18 (s, 1H), 1.54 (s, 8H) ppm.  $^{13}\text{C}$  NMR (126 MHz,  $\text{CDCl}_3$ )  $\delta$  180.0, 176.6, 170.4, 149.3, 144.0, 139.6, 135.6, 134.9, 132.8, 132.0, 129.9, 129.7, 126.9, 126.8, 125.1, 124.9, 123.0, 119.0, 115.4, 114.3, 83.9, 78.4, 72.0, 57.5, 30.5, 29.7, 29.3, 28.2 ppm. Mp. 109–111 °C. HRMS (DUIS):  $(\text{M} + \text{H})^+$  calcd. for  $\text{C}_{29}\text{H}_{27}\text{O}_5\text{N}_3\text{Cl}^+$ , 532.1639; found, 532.1599.

### 5.1.6. 2-((3-Chloro-1,4-dioxo-1,4-dihydronaphthalen-2-yl)amino)-3-(1*H*-indol-3-yl)-*N*-(prop-2-yn-1-yl)propanamide



In a round bottom flask *tert*-butyl (3-(1*H*-indol-3-yl)-1-oxo-1-(prop-2-yn-1-ylamino)propan-2-yl)(3-chloro-1,4-dioxo-1,4-dihydronaphthalen-2-yl)carbamate (100 mg, 0.2 mmol) was dissolved in 5 mL dichloromethane, and 1 mL trifluoroacetic acid was added, and the reaction mixture was stirred at RT. After 1 h 1 mL trifluoroacetic acid was added, and the mixture was stirred for 1 h at room temperature. The solvent was evaporated resulting in the product as a red foam (79 mg, 99%).  $^1\text{H}$  NMR (300 MHz,  $\text{CDCl}_3$ )  $\delta$  8.16 (s, 1H), 8.12 (d,  $J = 7.7$  Hz, 1H), 7.98 (d,  $J = 7.7$  Hz, 1H), 7.72 (t,  $J = 7.5$  Hz, 1H), 7.67 (d,  $J = 7.7$  Hz, 1H), 7.63 (t,  $J = 7.3$  Hz, 1H), 7.34 (d,  $J = 8.4$  Hz, 1H), 7.21–7.13 (m, 3H), 6.52–6.50 (m, 1H), 5.79–5.77 (m, 1H), 3.97 (dd,  $J = 5.4, 2.5$  Hz, 2H), 3.47 (dd,  $J = 14.6, 6.1$  Hz, 1H), 3.33 (dd,  $J = 14.5, 7.2$  Hz, 1H), 2.14 (t,  $J = 2.5$  Hz, 1H) ppm.  $^{13}\text{C}$  NMR (126 MHz,  $\text{CDCl}_3$ )  $\delta$  180.0, 176.8, 170.3, 149.1, 144.0, 139.9, 135.6, 135.0, 132.8, 132.2, 129.9, 129.7, 126.9, 126.8, 125.1, 124.9, 123.0, 119.0, 115.4, 114.3, 78.5, 72.0, 57.5, 30.4, 29.7, 29.2 ppm. Mp. 123 °C. HRMS (DUIS):  $(\text{M} + \text{H})^+$  calcd. for  $\text{C}_{24}\text{H}_{19}\text{O}_3\text{N}_3\text{Cl}^+$ , 432.1109; found, 432.1103.

### 5.1.7. 4-(vinylsulfonylamido)benzoic acid



4-Aminobenzoic acid (414 mg, 3 mmol), and triethylamine (0.57 mL, 3.6 mmol, 1.2 equiv.) was added to 20 mL dichloromethane and 10 mL THF at 0 °C. 2-Chloroethanesulfonyl chloride (0.35 mL, 3.3 mmol, 1.1 equiv.) was slowly added, and then the reaction mixture was stirred at 0 °C for 1 h. Triethylamine (0.77 mL, 4.5 mmol, 1.5 equiv.) was added, the reaction was stirred overnight, and then quenched with 10 mL 1 M HCl. After separation, the organic phase was dried over MgSO<sub>4</sub>, and the solvent was evaporated. The crude product was purified by flash column chromatography resulting in a pale-yellow solid (110 mg, 16%). <sup>1</sup>H NMR (300 MHz, DMSO-*d*<sub>6</sub>) δ 7.87 (d, *J* = 8.5 Hz, 2H), 7.22 (d, *J* = 8.5 Hz, 2H), 6.85 (dd, *J* = 16.4, 9.9 Hz, 1H), 6.21 (d, *J* = 16.4 Hz, 1H), 6.10 (d, *J* = 9.9 Hz, 1H) ppm. <sup>13</sup>C NMR (126 MHz, CDCl<sub>3</sub>) δ 167.4, 141.7, 136.6, 130.6, 129.7, 119.9, 118.5 ppm. Mp. 189 °C (lit. 195 °C) [66]. HRMS (DUI): (M + H)<sup>+</sup> calcd. for C<sub>9</sub>H<sub>10</sub>O<sub>4</sub>NS<sup>+</sup>, 228.0331; found, 228.0322.

## 6. Synthesis of peptides

With Fmoc chemistry, the peptide chain was elongated on TentaGel R RAM resin (0.18 mmol g<sup>-1</sup>). First, 3 equivalents of Fmoc-protected amino acid, 2.5 equivalents of the coupling agent ethyl cyanoglyoxylate-2-oxime (OxymaPure) and 3 equivalents of N,N-dicyclohexylcarbodiimide (DCC) were used in N,N-dimethylformamide (DMF) as solvent with shaking for 2 h. After the coupling step, the resin was washed 3 times with dichloromethane, once with MeOH and 3 times with dichloromethane. No truncated sequences were observed under these coupling conditions. Deprotection was performed with 2% 1,8-diazabicyclo[5.4.0]undec-7-ene (DBU) and 2% piperidine in DMF in two steps, with reaction times of 5 and 15 min. The resin was washed with the same solvents as described previously. The cleavage was performed with TFA/water/TIS (95:2.5:2.5) at 0 °C for 2 h.

The purification of peptides was carried out by RP-HPLC, using a Phenomenex Luna C18 100 Å 10 µm column (10 mm × 250 mm). The HPLC apparatus was made by JASCO. The solvent system used was as follows: 0.1% TFA in water; 0.1% TFA in 80% acetonitrile in water; a linear gradient was used during 60 min, at a flow rate of 4.0 mL min<sup>-1</sup>, with detection at 206 nm. The purities of the fractions were determined by analytical RP-HPLC using a JASCO HPLC system with a Phenomenex Luna C18 100 Å 5 µm column (4.6 mm × 250 mm) and the pure fractions were pooled and lyophilized. The purified peptides were characterized by HPLC-MS measurements, on a Bruker HCT Ultra ETD II mass spectrometer equipped with an Agilent 1260 HPLC.

### Declaration of competing interest

The authors declare that they have no known competing financial interests or personal relationships that could have appeared to influence the work reported in this paper.

### Acknowledgement

This research was funded by the European Union's Framework Programme for Research and Innovation Horizon 2020 (2014–2020) under the Marie Skłodowska-Curie grant agreement number ID 675899: FRAGment-based drug discovery NETwork

(FRAGNET) and by the National Brain Research Program (2017–1.2.1-NKP-2017-00002). P.Á.B. are grateful for the support of National Office of Research, Development and Innovation (OTKA PD124598). Technical support of K. Nyiri in the Ellman's assay and V. Varga in the syntheses are gratefully acknowledged.

## Appendix A. Supplementary data

Supplementary data to this article can be found online at <https://doi.org/10.1016/j.ejmech.2022.114163>.

## References

- [1] R.A. Bauer, Covalent inhibitors in drug discovery: from accidental discoveries to avoided liabilities and designed therapies, *Drug Discov. Today* 20 (9) (2015) 1061–1073, <https://doi.org/10.1016/j.drudis.2015.05.005>.
- [2] S.V. Singh, K. Singh, Cancer chemoprevention with dietary isothiocyanates mature for clinical translational research, *Carcinogenesis* 33 (10) (2012) 1833–1842, <https://doi.org/10.1093/carcin/bgs216>.
- [3] T.A. Baillie, Targeted covalent inhibitors for drug design, *Angew. Chem. Int. Ed.* 55 (43) (2016) 13408–13421, <https://doi.org/10.1002/anie.201601091>.
- [4] A.K. Ghosh, I. Samanta, A. Mondal, W.R. Liu, Covalent inhibition in drug discovery, *ChemMedChem* 14 (9) (2019) 889–906, <https://doi.org/10.1002/cmdc.201900107>.
- [5] D.A. Shannon, E. Weerapana, Covalent protein modification: the current landscape of residue-specific electrophiles, *Curr. Opin. Chem. Biol.* 24 (2015) 18–26, <https://doi.org/10.1016/j.cbpa.2014.10.021>.
- [6] B. Li, D. Rong, Y. Wang, Targeting protein-protein interaction with covalent small-molecule inhibitors, *Curr. Top. Med. Chem.* 19 (21) (2019) 1872–1876, <https://doi.org/10.2174/1568026619666191011163410>.
- [7] R. Nussinov, C.-J. Tsai, The design of covalent allosteric drugs, *Annu. Rev. Pharmacol. Toxicol.* 55 (1) (2015) 249–267, <https://doi.org/10.1146/annurev-pharmtox-010814-124401>.
- [8] A. Chen, A.N. Koehler, Transcription factor inhibition: lessons learned and emerging targets, *Trends Mol. Med.* 26 (5) (2020) 508–518, <https://doi.org/10.1016/j.molmed.2020.01.004>.
- [9] Z. Orgován, G.M. Keserü, Small molecule inhibitors of RAS proteins with oncogenic mutations, *Cancer Metastasis Rev.* 39 (4) (2020) 1107–1126, <https://doi.org/10.1007/s10555-020-09911-9>.
- [10] P. Tompa, Intrinsically unstructured proteins, *Trends Biochem. Sci.* 27 (10) (2002) 527–533, [https://doi.org/10.1016/S0968-0004\(02\)02169-2](https://doi.org/10.1016/S0968-0004(02)02169-2).
- [11] R. van der Lee, M. Buljan, B. Lang, R.J. Weatheritt, G.W. Daughdrill, A.K. Dunker, M. Fuxreiter, J. Gough, J. Gsponer, D.T. Jones, et al., Classification of intrinsically disordered regions and proteins, *Chem. Rev.* 114 (13) (2014) 6589–6631, <https://doi.org/10.1021/cr400525m>.
- [12] H.H. Nguyen, P. Ábrányi-Balogh, L. Petri, A. Mészáros, K. Pauwels, G. Vandenbussche, G.M. Keserü, P. Tompa, Targeting an Intrinsically Disordered Protein by Covalent Modification, 2020, pp. 835–854, [https://doi.org/10.1007/978-1-0716-0524-0\\_43](https://doi.org/10.1007/978-1-0716-0524-0_43).
- [13] M.E. Orr, A.C. Sullivan, B. Frost, A brief overview of tauopathy: causes, consequences, and therapeutic strategies, *Trends Pharmacol. Sci.* 38 (7) (2017) 637–648, <https://doi.org/10.1016/j.tips.2017.03.011>.
- [14] K. Iqbal, F. Liu, C.-X. Gong, I. Grundke-Iqbal, Tau in Alzheimer disease and related tauopathies, *Curr. Alzheimer Res.* 7 (8) (2010) 656–664, <https://doi.org/10.2174/156720510793611592>.
- [15] D.F.V. Pîrşcoveanu, I. Pirici, V. Tudorică, T.A. Bălşeanu, V.C. Albu, S. Bondari, A.M. Bumba, M. Pîrşcoveanu, Tau protein in neurodegenerative diseases - a review, *Rom. J. Morphol. Embryol.* 58 (4) (2017) 1141–1150.
- [16] G. Lippens, A. Sillen, I. Landrieu, L. Amniai, N. Sibille, P. Barbier, A. Leroy, X. Hanouille, J.-M. Wieruszkeski, Tau aggregation in Alzheimer's disease, *Prion* 1 (1) (2007) 21–25, <https://doi.org/10.4161/pr.1.1.4055>.
- [17] E. Tortosa, C. Montenegro-Venegas, M. Benoist, S. Härtel, C. González-Billault, J.A. Esteban, J. Avila, Microtubule-associated protein 1B (MAP1B) is required for dendritic spine development and synaptic maturation, *J. Biol. Chem.* 286 (47) (2011) 40638–40648, <https://doi.org/10.1074/jbc.M111.271320>.
- [18] M. von Bergen, S. Barghorn, L. Li, A. Marx, J. Biernat, E.-M. Mandelkow, E. Mandelkow, Mutations of tau protein in frontotemporal dementia promote aggregation of paired helical filaments by enhancing local β-structure, *J. Biol. Chem.* 276 (51) (2001) 48165–48174, <https://doi.org/10.1074/jbc.M105196200>.
- [19] M. von Bergen, P. Friedhoff, J. Biernat, J. Heberle, E.-M. Mandelkow, E. Mandelkow, Assembly of tau protein into Alzheimer paired helical filaments depends on a local sequence motif (306VQIVYK311) forming Beta structure, *Proc. Natl. Acad. Sci. Unit. States Am.* 97 (10) (2000) 5129–5134, <https://doi.org/10.1073/pnas.97.10.5129>.
- [20] N. Gustke, B. Trinczek, J. Biernat, E.-M. Mandelkow, E. Mandelkow, Domains of tau protein and interactions with microtubules, *Biochemistry* 33 (32) (1994) 9511–9522, <https://doi.org/10.1021/bi00198a017>.
- [21] D. Vagrys, J. Davidson, I. Chen, R.E. Hubbard, B. Davis, Exploring IDP–ligand interactions: tau K18 as a test case, *Int. J. Mol. Sci.* 21 (15) (2020) 5257, <https://doi.org/10.3390/ijms21155257>.

- [22] N. Gustke, B. Trinczek, J. Biernat, E.-M. Mandelkow, E. Mandelkow, Domains of tau protein and interactions with microtubules, *Biochemistry* 33 (32) (1994) 9511–9522, <https://doi.org/10.1021/bi00198a017>.
- [23] J. Yao, X. Gao, W. Sun, T. Yao, S. Shi, L. Ji, Molecular hairpin: a possible model for inhibition of tau aggregation by tannic acid, *Biochemistry* 52 (11) (2013) 1893–1902, <https://doi.org/10.1021/bi400240c>.
- [24] B. Bulic, M. Pickhardt, E. Mandelkow, Progress and developments in tau aggregation inhibitors for Alzheimer disease, *J. Med. Chem.* 56 (11) (2013) 4135–4155, <https://doi.org/10.1021/jm3017317>.
- [25] M. Silva, V. Caro, C. Guzmán, G. Perry, C. Areche, A.  $\alpha$ -Synuclein Cornejo, Tau, Two Targets for Dementia, 2020, pp. 1–25, <https://doi.org/10.1016/B978-0-12-819483-6.00001-1>.
- [26] D.J. Ingham, B.R. Blankenfeld, S. Chacko, C. Perera, B.R. Oakley, T.C. Gamblin, Fungally derived isoquinoline demonstrates inducer-specific tau aggregation inhibition, *Biochemistry* 60 (21) (2021) 1658–1669, <https://doi.org/10.1021/acs.biochem.1c00111>.
- [27] D. Malafaia, H.M.T. Albuquerque, A.M.S. Silva, Amyloid- $\beta$  and tau aggregation dual-inhibitors: a synthetic and structure-activity relationship focused review, *Eur. J. Med. Chem.* 214 (2021) 113209, <https://doi.org/10.1016/j.ejmech.2021.113209>.
- [28] S.R. Paranjape, Y.-M. Chiang, J.F. Sanchez, R. Entwistle, C.C.C. Wang, B.R. Oakley, T.C. Gamblin, Inhibition of tau aggregation by three *Aspergillus nidulans* secondary metabolites: 2, $\omega$ -dihydroxyemodin, asperthecin, and asperbenzaldehyde, *Planta Med.* 80 (1) (2014) 77–85, <https://doi.org/10.1055/s-0033-1360180>.
- [29] Y. Soeda, M. Yoshikawa, O.F.X. Almeida, A. Sumioka, S. Maeda, H. Osada, Y. Kondoh, A. Saito, T. Miyasaka, T. Kimura, et al., Toxic tau oligomer formation blocked by capping of cysteine residues with 1,2-dihydroxybenzene groups, *Nat. Commun.* 6 (1) (2015) 10216, <https://doi.org/10.1038/ncomms10216>.
- [30] M.M. Haque, D. Kim, Y.H. Yu, S. Lim, D.J. Kim, Y.-T. Chang, H.-H. Ha, Y.K. Kim, Inhibition of tau aggregation by a rosamine derivative that blocks tau intermolecular disulfide cross-linking, *Amyloid* 21 (3) (2014) 185–190, <https://doi.org/10.3109/13506129.2014.929103>.
- [31] R.C. George, J. Lew, D.J. Graves, Interaction of cinnamaldehyde and epicatechin with tau: implications of beneficial effects in modulating Alzheimer's disease pathogenesis, *J. Alzheim. Dis.* 36 (1) (2013) 21–40, <https://doi.org/10.3233/JAD-122113>.
- [32] C. González, C. Cartagena, L. Caballero, F. Melo, C. Areche, A. Cornejo, The fumarprotocetraric acid inhibits tau covalently, avoiding cytotoxicity of aggregates in cells, *Molecules* 26 (12) (2021) 3760, <https://doi.org/10.3390/molecules26123760>.
- [33] A. Dominguez-Mejide, E. Vasili, T.F. Outeiro, Pharmacological modulators of tau aggregation and spreading, *Brain Sci.* 10 (11) (2020) 858, <https://doi.org/10.3390/brainsci10110858>.
- [34] C. González-Bello, Designing irreversible inhibitors-worth the effort? *Chem-MedChem* 11 (1) (2016) 22–30, <https://doi.org/10.1002/cmdc.201500469>.
- [35] A.J.T. Smith, X. Zhang, A.G. Leach, K.N. Houk, Beyond picomolar affinities: quantitative aspects of noncovalent and covalent binding of drugs to proteins, *J. Med. Chem.* 52 (2) (2009) 225–233, <https://doi.org/10.1021/jm800498e>.
- [36] J.B. Fell, J.P. Fischer, B.R. Baer, J.F. Blake, K. Bouhana, D.M. Briere, K.D. Brown, L.E. Burgess, A.C. Burns, M.R. Burkard, et al., Identification of the clinical development candidate MRTX849, a covalent KRAS G12C inhibitor for the treatment of cancer, *J. Med. Chem.* 63 (13) (2020) 6679–6693, <https://doi.org/10.1021/acs.jmedchem.9b02052>.
- [37] E. Weerapana, C. Wang, G.M. Simon, F. Richter, S. Khare, M.B.D. Dillon, D.A. Bachovchin, K. Mowen, D. Baker, B.F. Cravatt, Quantitative reactivity profiling predicts functional cysteines in proteomes, *Nature* 468 (7325) (2010) 790–795, <https://doi.org/10.1038/nature09472>.
- [38] L.M. McGregor, M.L. Jenkins, C. Kerwin, J.E. Burke, K.M. Shokat, Expanding the scope of electrophiles capable of targeting K-ras oncogenes, *Biochemistry* 56 (25) (2017) 3178–3183, <https://doi.org/10.1021/acs.biochem.7b00271>.
- [39] M. Gersch, J. Kreuzer, S.A. Sieber, Electrophilic natural products and their biological targets, *Nat. Prod. Rep.* 29 (6) (2012) 659–682, <https://doi.org/10.1039/c2np20012k>.
- [40] J. Du, X. Yan, Z. Liu, L. Cui, P. Ding, X. Tan, X. Li, H. Zhou, Q. Gu, J. Xu, CBinderDB: a covalent binding agent database, *Bioinformatics* 33 (8) (2017) 1258–1260, <https://doi.org/10.1093/bioinformatics/btw801>.
- [41] P. Ábrányi-Balogh, L. Petri, T. Imre, P. Szijj, A. Scarpino, M. Hrast, A. Mitrović, U.P. Fonović, K. Németh, H. Barreteau, et al., A road map for prioritizing warheads for cysteine targeting covalent inhibitors, *Eur. J. Med. Chem.* 160 (2018) 94–107, <https://doi.org/10.1016/j.ejmech.2018.10.010>.
- [42] A. Keeley, L. Petri, P. Ábrányi-Balogh, G.M. Keserű, Covalent fragment libraries in drug discovery, *Drug Discov. Today* 25 (6) (2020) 983–996, <https://doi.org/10.1016/j.drudis.2020.03.016>.
- [43] L. Petri, P. Ábrányi-Balogh, I. Tímea, G. Pálffy, A. Perczel, D. Knez, M. Hrast, M. Gobec, I. Sosić, K. Nyíri, et al., Assessment of tractable cysteines for covalent targeting by screening covalent fragments, *Chembiochem* 22 (4) (2021) 743–753, <https://doi.org/10.1002/cbic.202000700>.
- [44] L. Petri, A. Egyed, D. Bajusz, T. Imre, A. Hetényi, T. Martinek, P. Ábrányi-Balogh, G.M. Keserű, An electrophilic warhead library for mapping the reactivity and accessibility of tractable cysteines in protein kinases, *Eur. J. Med. Chem.* 207 (2020) 112836, <https://doi.org/10.1016/j.ejmech.2020.112836>.
- [45] D.G. Hoch, D. Abegg, A. Adibekian, Cysteine-reactive probes and their use in chemical proteomics, *Chem. Commun.* 54 (36) (2018) 4501–4512, <https://doi.org/10.1039/C8CC01485J>.
- [46] B. Bulic, M. Pickhardt, I. Khlistunova, J. Biernat, E.-M. Mandelkow, E. Mandelkow, H. Waldmann, Rhodanine-based tau aggregation inhibitors in cell models of tauopathy, *Angew. Chem. Int. Ed.* 46 (48) (2007) 9215–9219, <https://doi.org/10.1002/anie.200704051>.
- [47] B. Falcon, J. Zivanov, W. Zhang, A.G. Murzin, H.J. Garringer, R. Vidal, R.A. Crowther, K.L. Newell, B. Ghetti, M. Goedert, et al., Novel tau filament fold in chronic traumatic encephalopathy encloses hydrophobic molecules, *Nature* 568 (7752) (2019) 420–423, <https://doi.org/10.1038/s41586-019-1026-5>.
- [48] P.M. Seidler, D.R. Boyer, J.A. Rodriguez, M.R. Sawaya, D. Cascio, K. Murray, T. Gonen, D.S. Eisenberg, Structure-based inhibitors of tau aggregation, *Nat. Chem.* 10 (2) (2018) 170–176, <https://doi.org/10.1038/nchem.2889>.
- [49] K. Bhattacharya, K.B. Rank, D.B. Evans, S.K. Sharma, Role of cysteine-291 and cysteine-322 in the polymerization of human tau into Alzheimer-like filaments, *Biochem. Biophys. Res. Commun.* 285 (1) (2001) 20–26, <https://doi.org/10.1006/bbrc.2001.5116>.
- [50] B. Bulic, M. Pickhardt, I. Khlistunova, J. Biernat, E.-M. Mandelkow, E. Mandelkow, H. Waldmann, Rhodanine-based tau aggregation inhibitors in cell models of tauopathy, *Angew. Chem. Int. Ed.* 46 (48) (2007) 9215–9219, <https://doi.org/10.1002/anie.200704051>.
- [51] S. Giorgetti, C. Greco, P. Tortora, F. Aprile, Targeting amyloid aggregation: an overview of strategies and mechanisms, *Int. J. Mol. Sci.* 19 (9) (2018) 2677, <https://doi.org/10.3390/ijms19092677>.
- [52] X. Chen, J.L. Zaro, W.-C. Shen, Fusion protein linkers: property, design and functionality, *Adv. Drug Deliv. Rev.* 65 (10) (2013) 1357–1369, <https://doi.org/10.1016/j.addr.2012.09.039>.
- [53] R. Arai, H. Ueda, A. Kitayama, N. Kamiya, T. Nagamune, Design of the linkers which effectively separate domains of a bifunctional fusion protein, *Protein Eng. Des. Sel.* 14 (8) (2001) 529–532, <https://doi.org/10.1093/protein/14.8.529>.
- [54] Y. Chen, M.T. Kim, L. Zheng, G. Deperalta, F. Jacobson, Structural characterization of cross-linked species in trastuzumab emtansine (kadcyla), *Bioconjugate Chem.* 27 (9) (2016) 2037–2047, <https://doi.org/10.1021/acs.bioconjchem.6b00316>.
- [55] H.L. Zhao, X.Q. Yao, C. Xue, Y. Wang, X.H. Xiong, Z.M. Liu, Increasing the homogeneity, stability and activity of human serum albumin and interferon- $\alpha$ 2b fusion protein by linker engineering, *Protein Expr. Purif.* 61 (1) (2008) 73–77, <https://doi.org/10.1016/j.pep.2008.04.013>.
- [56] E. Atherton, R.C. Sheppard, Solid phase peptide synthesis using N  $\alpha$ -fluorenylmethoxycarbonylamino acid pentafluorophenyl esters, *J. Chem. Soc., Chem. Commun.* 3 (1985) 165–166, <https://doi.org/10.1039/C39850000165>.
- [57] P.M. Seidler, D.R. Boyer, J.A. Rodriguez, M.R. Sawaya, D. Cascio, K. Murray, T. Gonen, D.S. Eisenberg, Structure-based inhibitors of tau aggregation, *Nat. Chem.* 10 (2) (2018) 170–176, <https://doi.org/10.1038/nchem.2889>.
- [58] S.L. Shammass, G.A. Garcia, S. Kumar, M. Kjaergaard, M.H. Horrocks, N. Shivji, E. Mandelkow, T.P.J. Knowles, E. Mandelkow, D. Klenerman, A mechanistic model of tau amyloid aggregation based on direct observation of oligomers, *Nat. Commun.* 6 (1) (2015) 7025, <https://doi.org/10.1038/ncomms8025>.
- [59] K. Gade Malmos, L.M. Blancas-Mejia, B. Weber, J. Buchner, M. Ramirez-Alvarado, H. Naiki, D. Otzen, ThT 101: a primer on the use of Thioflavin T to investigate amyloid formation, *Amyloid* 24 (1) (2017) 1–16, <https://doi.org/10.1080/13506129.2017.1304905>.
- [60] J. Biernat, N. Gustke, G. Drewes, E.-M. Mandelkow, E. Mandelkow, Phosphorylation of Ser262 strongly reduces binding of tau to microtubules: distinction between PHF-like immunoreactivity and microtubule binding, *Neuron* 11 (1) (1993) 153–163, [https://doi.org/10.1016/0896-6273\(93\)90279-2](https://doi.org/10.1016/0896-6273(93)90279-2).
- [61] ProteinProspector, retrieved on 20/05/2020, <http://Prospector.Ucsf.Edu/Prospector/Mshome.Htm>.
- [62] C.J. Huseby, J. Kuret, Analyzing Tau Aggregation with Electron Microscopy, 2016, pp. 101–112, [https://doi.org/10.1007/978-1-4939-2978-8\\_7](https://doi.org/10.1007/978-1-4939-2978-8_7).
- [63] L. Al-Riyami, M.A. Pineda, J. Rzepecka, J.K. Huggan, A.I. Khalaf, C.J. Suckling, F.J. Scott, D.T. Rodgers, M.M. Harnett, W. Harnett, Designing anti-inflammatory drugs from parasitic worms: a synthetic small molecule analogue of the acanthocheilonema viteae product ES-62 prevents development of collagen-induced arthritis, *J. Med. Chem.* 56 (24) (2013) 9982–10002, <https://doi.org/10.1021/jm401251p>.
- [64] D.A. Alonso, C. Nájera, M. Varea,  $\pi$ -Deficient 2-(Arylsulfonyl)Ethyl Esters as Protecting Groups for Carboxylic Acids, *Synthesis*, 2003, <https://doi.org/10.1055/s-2003-36844>.
- [65] S. Córdova-Rivas, J.G. Araujo-Huitrardo, E. Rivera-Avalos, I.L. Escalante-García, S.M. Durón-Torres, Y. López-Hernández, H. Hernández-López, L. López, D. de Loera, J.A. López, Differential proliferation effect of the newly synthesized valine, tyrosine and tryptophan-naphthoquinones in immortal and tumorigenic cervical cell lines, *Molecules* 25 (9) (2020) 2058, <https://doi.org/10.3390/molecules25092058>.
- [66] E. Friedrich, A.G. Basf, Verfahren Zur Herstellung von Aethensulfarylamiden, Germany, 1952, p. DE832149. C.